Pergamon

Geochimica et Cosmochimica Acta, Vol. 65, No. 6, pp. 847–869, 2001

0016-7037/01 $20.00 + .00

PII S0016-7037(00)00577-9

Differential rates of feldspar weathering in granitic regoliths

ART F. WHITE,[1] THOMAS D. BULLEN,[1] MARJORIE S. SCHULZ,[1] ALEX E. BLUM,[2] THOMAS G. HUNTINGTON,[3] and NORMAN E. PETERS[3]

[1]U.S. Geological Survey, Menlo Park, California 94025, USA
[2]U.S. Geological Survey, Boulder, Colorado 80303, USA
[3]U.S. Geological Survey, Atlanta, Georgia 30360, USA

(*Received May* 16, 2000; *accepted in revised form October* 10, 2000)

Abstract—Differential rates of plagioclase and K-feldspar weathering commonly observed in bedrock and soil environments are examined in terms of chemical kinetic and solubility controls and hydrologic permeability. For the Panola regolith, in the Georgia Piedmont Province of southeastern United States, petrographic observations, coupled with elemental balances and $^{87}Sr/^{86}Sr$ ratios, indicate that plagioclase is being converted to kaolinite at depths $>$ 6 m in the granitic bedrock. K-feldspar remains pristine in the bedrock but subsequently weathers to kaolinite at the overlying saprolite. In contrast, both plagioclase and K-feldspar remain stable in granitic bedrocks elsewhere in Piedmont Province, such as Davis Run, Virginia, where feldspars weather concurrently in an overlying thick saprolite sequence. Kinetic rate constants, mineral surface areas, and secondary hydraulic conductivities are fitted to feldspar losses with depth in the Panola and Davis Run regoliths using a time-depth computer spreadsheet model. The primary hydraulic conductivities, describing the rates of meteoric water penetration into the pristine granites, are assumed to be equal to the propagation rates of weathering fronts, which, based on cosmogenic isotope dating, are 7 $m/10^6$ yr for the Panola regolith and 4 $m/10^6$ yr for the Davis Run regolith. Best fits in the calculations indicate that the kinetic rate constants for plagioclase in both regoliths are factors of two to three times faster than K-feldspar, which is in agreement with experimental findings. However, the range for plagioclase and K-feldspar rates ($k_r = 1.5 \times 10^{-17}$ to 2.8×10^{-16} mol m^{-2} s^{-1}) is three to four orders of magnitude lower than for that for experimental feldspar dissolution rates and are among the slowest yet recorded for natural feldspar weathering. Such slow rates are attributed to the relatively old geomorphic ages of the Panola and Davis Run regoliths, implying that mineral surface reactivity decreases significantly with time.

Differential feldspar weathering in the low-permeability Panola bedrock environment is more dependent on relative feldspar solubilities than on differences in kinetic reaction rates. Such weathering is very sensitive to primary and secondary hydraulic conductivities (q_p and q_s), which control both the fluid volumes passing through the regolith and the thermodynamic saturation of the feldspars. Bedrock permeability is primarily intragranular and is created by internal weathering of networks of interconnected plagioclase phenocrysts. Saprolite permeability is principally intergranular and is the result of dissolution of silicate phases during isovolumetric weathering. A secondary to primary hydraulic conductivity ratio of $q_s/q_p = 150$ in the Panola bedrock results in kinetically controlled plagioclase dissolution but thermodynamically inhibited K-feldspar reaction. This result is in accord with calculated chemical saturation states for groundwater sampled in the Panola Granite. In contrast, greater secondary conductivities in the Davis Run saprolite, $q_s/q_p = 800$, produces both kinetically controlled plagioclase and K-feldspar dissolution. Faster plagioclase reaction, leading to bedrock weathering in the Panola Granite but not at Davis Run, is attributed to a higher anorthite component of the plagioclase and a wetter and warmer climate. In addition, the Panola Granite has an abnormally high content of disseminated calcite, the dissolution of which precedes the plagioclase weathering front, thus creating additional secondary permeability.

1. INTRODUCTION

Quantification of silicate weathering rates has important implications in a diverse range of geochemical issues. Among them are rates of neutralization of acid precipitation via silicate hydrolysis reactions (Stauffer, 1990), the rates of release of macronutrients such as K and Ca in forested catchments (Huntington et al., 2000), and the linkage between weathering rates and CO_2 draw-down and long-term climate change (Berner and Berner, 1997). Toward addressing these issues, extensive efforts have been directed at determining reaction mechanisms and rates of plagioclase and K-feldspar weathering, two of the most common minerals present in crystalline protoliths (Blum and Stillings, 1995, and references therein).

Despite these efforts, discrepancies remain between laboratory and field findings. Commonly, estimated field weathering rates of feldspar are two to four orders of magnitude slower than laboratory dissolution rates (Brantley, 1992; White et al., 1996). In addition, laboratory reaction rates for sodic plagioclase are only a factor of two to three times faster than K-feldspar rates at near-neutral pHs (Blum and Stillings, 1995 and references therein). These data contradict commonly observed field situations in which plagioclase feldspar exhibits more intense weathering features and is significantly depleted in regoliths relative to K-feldspar (Banfield and Eggleton, 1990; Nesbitt et al., 1997). Possible reasons for differences in both relative and absolute rates of feldspar weathering include differences in physical and reactive surface areas and defect densities (White and Peterson, 1990;

*Author to whom correspondence should be addressed (afwhite@usgs.gov).

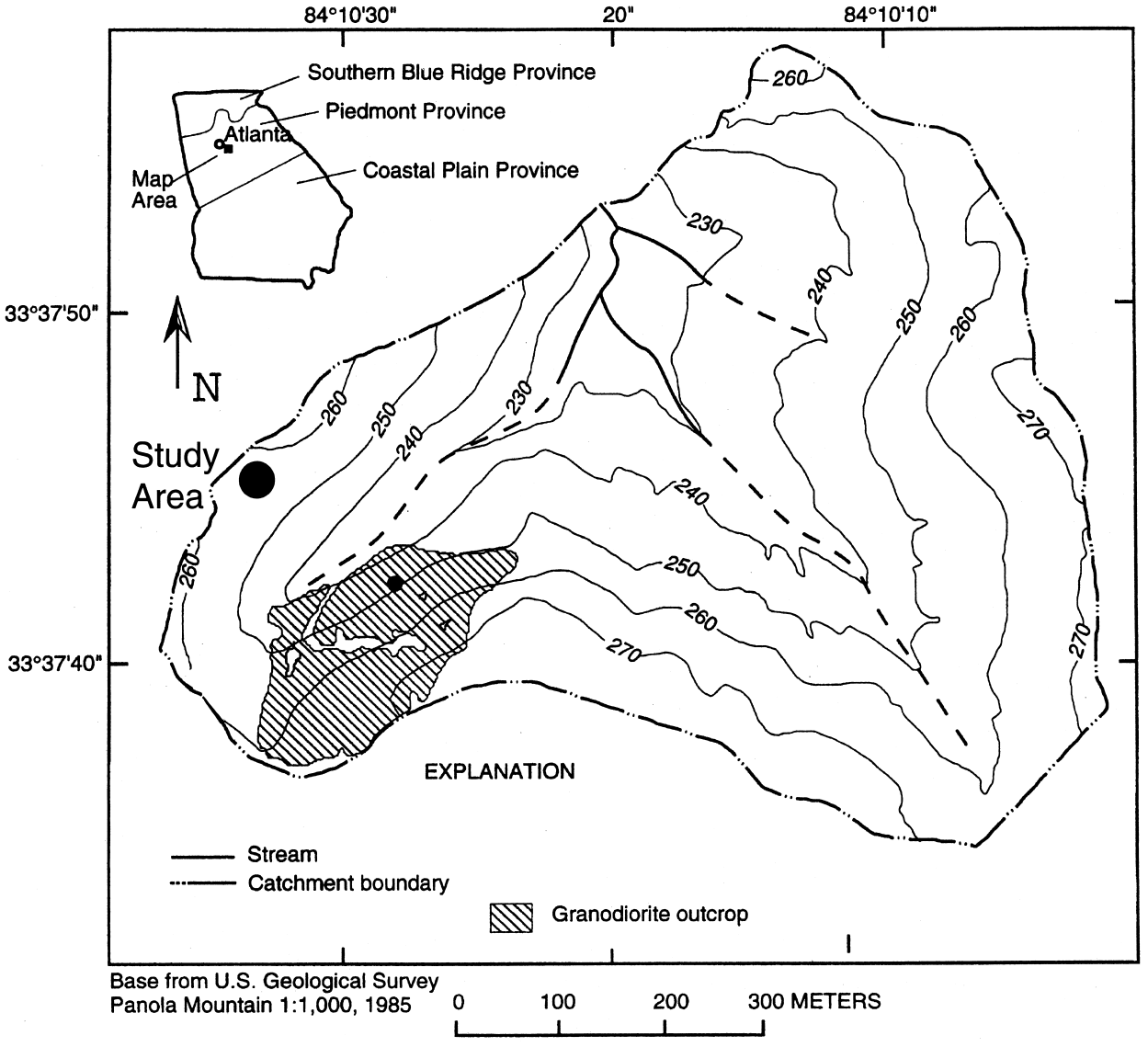

Fig. 1. Location map of the Panola Watershed and regolith study area.

Brantley et al., 1999), impacts of aqueous chemical species and concentrations on reaction affinities (Burch et al., 1993; Oelkers et al., 1994), and the role of hydrology in determining mineral surface wetting and solute transport (Swodoba-Colberg and Drever, 1992; Clow and Drever, 1996).

The present study addresses how differing weathering environments control natural feldspar weathering rates in granitic regoliths. The work focuses on well-characterized weathering profiles consisting of thick soil-saprolite sequences developed on crystalline bedrock in the Piedmont Province of southeastern United States (Gardner, 1980; Calvert et al., 1980; Pavich, 1986; Cleaves, 1993). These regoliths are geomorphically old ($>10^5$ yr), are developed in situ from granitic bedrock, and have undergone isovolumetric weathering involving significant mass losses. These features make for long-term steady-state conditions optimal for characterizing chemical weathering. Detailed elemental and $^{87}Sr/^{86}Sr$ distributions and petrologic data are presented for the Panola regolith in Georgia. Mass balance calculations are used to construct plagioclase and K-feldspar distributions in the Panola regolith that are then compared with significantly different feldspar distributions in other Piedmont regoliths. Feldspar saturation states are determined on the basis of pore and groundwater chemical compositions. Finally, a spreadsheet model is presented that uses kinetic rate constants, surface areas, and primary and secondary fluid conductivities to explain both absolute and relative differences in plagioclase and K-feldspar weathering rates.

2. FIELD SETTING AND METHODOLGIES

Detailed weathering studies are conducted within Panola Mountain Research Watershed located in the Piedmont province of eastern United States, 25 km southeast of Atlanta, Georgia (Fig. 1). Previous chemical weathering studies involving the Panola watershed include Grant (1975), Nixon (1981), Burns (1998), Stonestrom et al. (1998), Schroeder and Melear (1999), White et al. (1999a,b), and White et al. (2001). The relief in the catchment is 56 m with flat ridge tops and generally steep hill slopes. The regolith discussed in the present study

is situated on a ridge top site in the southwestern quadrant of the watershed and is underlain by the 320 myr-old Panola Granite described as a biotite-muscovite-oligioclase-quartz-microcline granodiorite (Higgins et al., 1988). Bierman et al. (1995) measured ^{36}Cl concentrations in surface outcrops of granodiorite within the Panola watershed and calculated exposure ages of between 250 and 500 kyr. These distributions produced a mean model erosion rate of 7 m myr^{-1}, which is in agreement with steady-state chemical weathering rates calculated from solute fluxes (White et al., 2001).

The ridge topsoils in the Panola watershed are highly weathered ultisols developed from bedrock residuum. Soils consist of a dense dark red unstructured clay-rich A-horizon (~0.5 m thick), underlain by a less dense orange-brown B-horizon (~1 m thick). The in situ nature of weathering in these soils is confirmed by the remnants of small tourmaline-containing aplite dikes identical to those contained in granodiorite exposures in the watershed. The B-horizon is also cut by small horizontal and vertical fractures containing homogeneous clay material that precipitated along preferential flow paths and/or that was deposited as a result of physical translocation from the overlying A horizon. The soils are underlain by a porous gray saprolite (3–4 m thick) that retains the original granodiorite texture. The saprolite-bedrock interface grades from friable saprock to competent bedrock over an interval of several centimeters. The depth of this bedrock interface is variable along the ridge top. Drilling confirmed that the bedrock is cut by numerous fractures.

Regolith samples were obtained by augering to the saprolite-bedrock interface (4.6 m). A bedrock core was obtained to a total depth of 16 m by using diamond bit drilling. Nested porous cup suction water samplers were installed at selective depths at the bottom of augered holes in the soil and saprolite and were sampled on a biweekly to monthly schedule from December 1991 to April 1995. Pore waters were also sampled from two additional sites on the upper and lower hill slope. More detailed discussions of Panola regolith hydrology and solute compositions are presented elsewhere (Burns, 1998; Stonestrom et al., 1998; White et al., 2001).

Selected regolith samples were powdered and run for whole rock analysis by using X-ray fluorescence spectrometry and X-ray diffraction analysis. Thin sections were prepared and characterized by using an electron microprobe and scanning electron microscopy. Individual mineral fractions were obtained by using magnetic and heavy liquid separation and hand sorting. $^{87}Sr/^{86}Sr$ ratios were determined by thermal ionization using a Finnigan-MAT 261 mass spectrometer. Solute alkalinity and pH were measured in the laboratory. Anions were analyzed for using ion chromatography and cations measured by using direct-coupled plasma optical emission spectroscopy.

Weathering intensities of elements and minerals in this study are described in terms of their compositions relative to the initial unweathered granitoid. The quantitative gains or losses of an element or mineral j can be obtained from the concentration of the weathered component $C_{j,w}$ ratioed against the corresponding concentration in the underlying unweathered protolith $C_{j,p}$. This ratio is dependent on three parameters as defined in Eqn. 1 (Brimhall and Dietrich, 1987).

$$\frac{C_{j,w}}{C_{j,p}} = \frac{\rho_p}{\rho_w} \frac{1}{(\varepsilon_i + 1)} (1 + \tau_j) \quad (1)$$

The ratio of the density change, ρ_p/ρ_w, is associated with the dissolution and precipitation of mobile elements. The volume ratio V_w/V_p, resulting from soil compaction or extension, is described by the strain factor $1/(\epsilon_{i+1})$ where $\epsilon_i = V_w/V_p - 1$. Together, density and volume changes describe closed system contributions that occur without movement of the component under consideration (i.e., $C_{j,w}$). The mass transport coefficient τ_j is an open system contribution that describes the mobility of component j within a unit volume of regolith. The above parameters have been used to evaluate weathering rates in a number of environments (Chadwick et al., 1990; Brimhall et al., 1991; White et al., 1996).

The volumetric strain or volume change can be calculated from the ratios of densities and concentrations of an inert element or mineral i in the soil and protolith (Eqn. 2) to give

$$\varepsilon_i = \frac{\rho_p C_{i,p}}{\rho_w C_{i,w}} - 1 \quad (2)$$

Positive values of ϵ_i indicate regolith expansion and negative values indicate collapse. A value of $\epsilon_i \approx 0$ is indicative of isovolumetric weathering.

Finally, elemental mobilities during regolith weathering are characterized by the mass transfer coefficients τ_j (Eqn. 3), which are computed from density and chemical composition data in combination with volume change derived from the strain calculations

$$\tau_j = \frac{\rho_w C_{j,w}}{\rho_p C_{j,p}} (\varepsilon_i + 1) - 1 \quad (3)$$

When $\tau_j = -1$, element j is completely removed during weathering. If $\tau_j = 0$, the element is immobile during weathering with respect to the volume of regolith considered.

3. RESULTS

3.1. Isovolumetric Weathering

The extent of volume change during weathering is critical in determining element mobilities and regolith permeabilities. Volume changes are determined from the ratios of the bulk densities in the protolith and regolith and from the concentrations of inert conservative chemical species (Eqn. 2). The density ratios ρ_p/ρ_w are calculated directly from the bulk density measurements in the weathered regolith and the fresh granodiorite (Table 1). Conservative elements most often used in Eqn. 2 include Zr (Harden, 1987; Chadwick et al., 1990), Ti (Johnson et al., 1968), and rare earth elements such as Nb (Brimhall and Dietrich, 1987). Although such elements are generally inert during weathering, conservative behavior under any specific geochemical condition is not guaranteed. For example, Gardner (1980) found that Ti was mobilized in a saprolite sequence on granite in the Piedmont Province of South Carolina, United States. Therefore, the best strategy is to use a suite of inert elements (Ti, Zr, and Nb tabulated in Table 1) to establish the extent of volumetric changes during soil weathering (White, 1995).

Except for the shallowest soils, which may have undergone volume increases due to bioturbation and the introduction of organic matter, volume changes defined in terms of ϵ_i (Eqn. 2), calculated from Zr, Ti, and Nb concentrations in the regolith, all center close to zero, indicating that weathering is essentially isovolumetric (Fig. 2A). This is in agreement with the preservation of primary granitic textures in the saprolite with average porosities of nearly 35%. Isovolumetric weathering is commonly observed for saprolites developed on granites and gneisses in the Piedmont of southeastern United States (Gardner, 1980; Markewich and Pavich, 1991; Cleaves, 1993). Petrographic evidence from the Panola saprolite is consistent with processes that preserve regolith volume. These include differential rates of mineral weathering, the formation of "boxwork" textures by secondary minerals surrounding primary mineral grains and etch-pit formation that produces "sponge-like" residual primary mineral grains (Velbel, 1990).

3.2. Elemental Distributions and Mobilities

Chemical data for the ridge top regolith tabulated in Table 1 are plotted vs. depth in Figure 3. Na and Ca are strongly depleted in the weathered bedrock (4.5–9.5 m) compared with the fresh bedrock (>10.5 m). Si concentrations decrease slightly in the weathered bedrock and saprolite and increase sharply in the upper soil horizon. K and Mg concentrations

Table 1. Depth, densities, and elemental and isotopic compositions of the Panola regolith.

Sample	Depth (m)	Density (g cm^{-3})	SiO_2 (wt.%)	Al_2O_3 (wt.%)	Fe_2O_3 (wt.%)	MgO (wt.%)	CaO (wt.%)	Na_2O (wt.%)	K_2O (wt.%)	TiO_2	Zr (ppm)	Nb (ppm)	Sr (ppm)	$^{87}Sr/^{86}Sr$
"A" soil	0.10	2.34	81.1	8.8	2.74	0.21	0.14	0.44	3.05	1.91	1525	26	163	0.71602
"B" soil	0.30	1.86	77.7	11.8	3.12	0.31	0.12	0.35	3.40	1.50	984	27	169	nd
	0.48	1.86	64.0	19.9	5.83	0.50	0.11	0.31	2.81	1.38	589	27	149	nd
	0.74	1.83	60.4	21.1	6.37	0.39	0.07	0.25	3.05	1.07	453	27	168	nd
	0.84	1.73	59.9	21.7	6.76	0.44	0.06	0.23	2.63	1.21	516	29	175	nd
	1.07	1.81	63.7	20.9	6.60	0.49	0.06	0.20	2.52	1.26	549	27	209	0.71530
	1.27	1.83	60.3	22.3	6.95	0.48	0.06	0.20	2.61	1.16	458	27	237	0.71868
	1.52	1.78	58.9	22.1	7.08	0.45	0.06	0.22	2.14	1.08	424	25	210	nd
Saprolite	1.83	1.80	61.3	22.1	7.13	0.39	0.05	0.16	2.65	1.20	473	27	258	0.71981
	2.16	1.72	61.7	23.1	6.18	0.53	0.06	0.19	3.15	1.21	491	26	342	0.71560
	2.51	1.99	62.6	22.1	6.58	0.74	0.06	0.14	3.20	1.31	505	28	377	0.71570
	2.84	2.25	66.0	20.6	6.05	0.81	0.07	0.23	4.41	1.33	649	27	312	0.71630
	3.23	1.97	69.8	16.7	6.26	1.18	0.06	0.21	4.93	1.49	688	29	274	0.71550
	3.73	2.00	65.5	21.4	5.31	1.06	0.05	0.20	4.01	1.22	572	23	269	0.71650
	3.99	1.98	65.7	19.7	5.68	0.98	0.05	0.22	4.18	1.27	473	25	319	0.71640
	4.29	1.92	63.6	21.0	4.80	0.90	0.05	0.23	3.06	1.00	482	24	200	0.71625
	4.52	1.98	67.4	19.1	5.39	0.92	0.07	0.21	3.96	1.27	566	26	432	0.71580
	4.65	2.00	69.4	18.4	5.32	1.09	0.06	0.20	4.13	1.26	598	25	339	0.71680
	4.79	1.93	60.9	18.7	4.95	1.10	0.08	0.47	5.48	1.08	725	23	324	0.71501
Weathered granodiorite	6.69	1.83	65.5	15.4	5.39	1.27	0.06	0.42	5.86	1.16	758	23	248	0.71846
	6.99	1.83	64.2	16.4	4.89	1.14	0.01	0.29	5.92	1.11	746	27	261	0.71727
	7.30	1.81	65.3	14.6	5.83	1.35	0.08	0.54	5.87	1.22	817	25	191	0.72117
	7.75	1.83	66.2	14.9	5.57	1.28	0.13	0.60	5.63	1.19	762	25	223	0.71910
	8.66	1.78	64.9	15.6	4.68	1.09	0.96	2.36	5.01	1.02	680	21	264	0.71641
	9.27	2.25	65.2	15.2	4.78	1.11	1.33	2.51	4.90	1.05	675	20	271	0.71553
	9.88	2.31	65.4	15.2	4.69	1.11	1.39	2.17	4.83	1.02	673	24	262	0.71580
	10.18	2.65	66.6	15.0	4.38	0.99	1.50	2.88	4.66	0.94	632	17	296	0.71523
	10.34	2.65	66.9	14.8	4.34	0.97	1.98	3.23	4.51	0.91	668	18	313	0.71425
Fresh granodiorite	10.49	2.65	68.8	14.9	4.29	0.93	1.88	3.31	4.55	0.87	632	23	259	0.71406
	10.64	2.65	66.5	14.8	4.13	1.01	2.21	3.21	4.62	0.94	597	19	325	0.71477
	10.94	2.65	66.5	14.8	4.86	1.13	2.09	3.20	4.53	1.00	676	18	324	0.71557
	11.55	2.65	66.5	14.7	4.34	1.01	2.41	3.16	4.75	0.90	642	18	231	0.71580

n.d. = not determined.

increase in the weathered bedrock relative to the fresh granodiorite but decrease in the overlying saprolite and soil. Fe and Al increase in the upper bedrock and saprolite but decrease in the soil, particularly in the shallowest A horizon.

The extent of elemental mobility in the regolith relative to the initial granodiorite composition is defined in terms of τ_j (Eqn. 3). The calculations assume that Ti is conservative. Values of τ_j for the major elements values cluster near zero in the bedrock below 10.5 m, indicating a lack of element mobility (Fig. 2B,C). In contrast, Ca is almost completely mobilized at depths of between 4.5 and 10.5 m in the weathered bedrock (τ_{Ca} decreases from -0.10 to -0.96), Na is also strongly mobilized (τ_{Na} decreases from -0.15 to -0.85) and Si is moderately mobilized ($\tau_{Si} < -0.25$). Weathering is highly selective because K, Mg, Al, and Fe remain essentially immobile in the upper bedrock ($\tau_j \cong 0$). K exhibits a sharp increase in mobility in the saprolite directly above the weathered bedrock interface (4.5 m), where τ_K decreases from 0.03 to -0.32 (Fig. 2B). The loss of K continues upward into saprolite and soil. The loss of Mg is much less near the bedrock/saprolite interface (τ_{Mg} decreases from -0.02 to -0.20). However, Mg decreases more rapidly than K upward in the saprolite and is essentially depleted in the soil A horizon ($\tau_{Mg} = -0.89$ at 0.1 m). Fe and Al are also strongly depleted in the upper A soil horizon ($\tau_{Fe} = -0.67$ and $\tau_{Al} = -0.70$ at 0.1 m) but are significantly enriched relative to fresh bedrock concentrations in the B-horizon and in the upper saprolite (Fig. 2C). This distribution is indicative of downward Fe and Al mobilization and subsequent reprecipitation.

The element distributions described above denote sequential weathering as fresh bedrock is first converted to weathered bedrock, then to saprolite, and finally to soil. The total elemental mass loss or gain ΔM_j (mol) over depth Δz (m) during each of these conversions, normalized to unit regolith surface area (m^2), is calculated from the expression (Chadwick et al., 1990; White et al., 1996)

$$\Delta M_{j,1} = \left(\rho_p \frac{C_{j,p}}{m_j} 10^4\right) \int_0^z - (\tau_j) dz \qquad (4)$$

ρ_p is density (g cm^{-3}) and m_j is the atomic weight of element (mol g^{-1}). The highlighted data in Table 2 indicate that Ca, Na, and Si are strongly mobilized during bedrock weathering. Subsequently, most of the Mg and K are lost during the conversion of weathered bedrock to saprolite, and finally Fe and Al are mobilized during the conversion of saprolite to soil.

3.3. Mineral Distributions and Weathering

Average mineralogy of the fresh Panola granodiorite, determined from point counts (Table 3), indicate a preponderance of plagioclase (32%), quartz (28%), K feldspar (21%), biotite

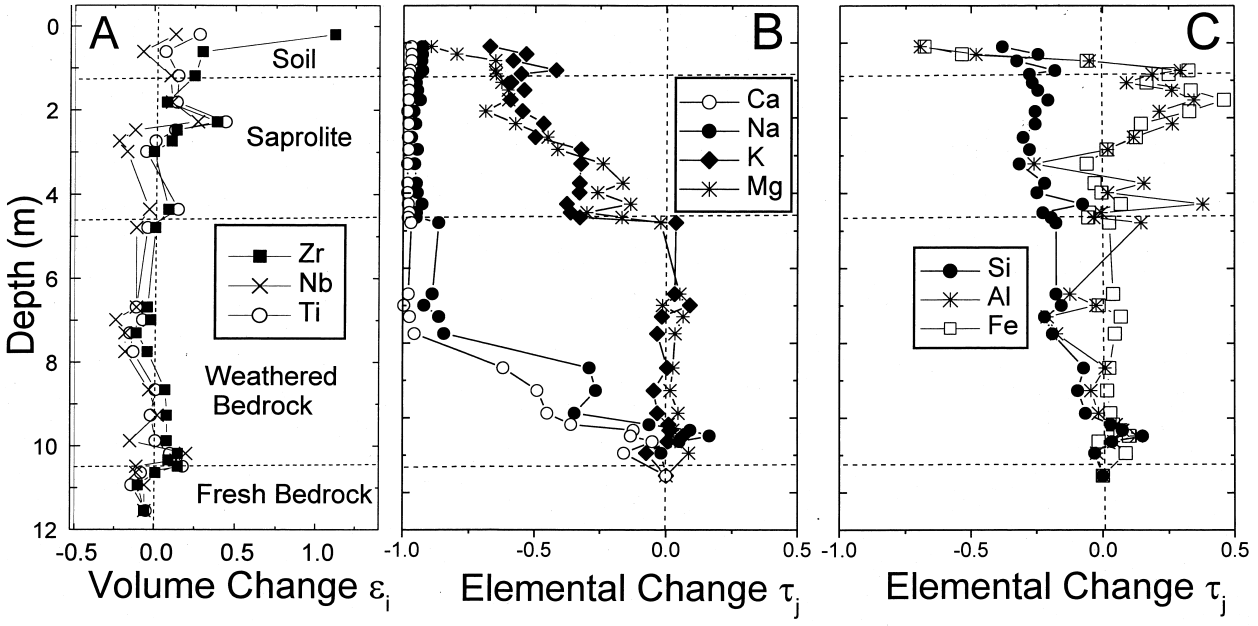

Fig. 2. Volume changes and elemental mass transfers within the Panola regolith. (A) Volumetric changes. Compaction and dilation are denoted by values of $\epsilon_i < 0$ and $\epsilon_i > 0$, respectively. A value of $\epsilon_i = 0$ denotes isovolumetric weathering. (B) Changes in Ca, Na, K, and Mg with regolith depth. (C) Changes in Si, Al, and Fe with regolith depth. A value $\tau_j = 0$ denotes no elemental loss and a value of $\tau_j = -1$ denotes complete elemental loss.

(13%), and muscovite (7%) with much lesser amounts of hornblende (<2%, not included in Table 3). Accessory minerals include apatite, zircon, and calcite. Plagioclase compositions in fresh granodiorite, as determined by microprobe analysis, range between An_{16} and An_{27} with an average of An_{23}. K-feldspar compositions range between Ab_2 and Ab_4 with an average of Ab_{31}. Petrographic observations and microprobe analyses did not detect significant exsolution features or perthitic textures in the feldspars.

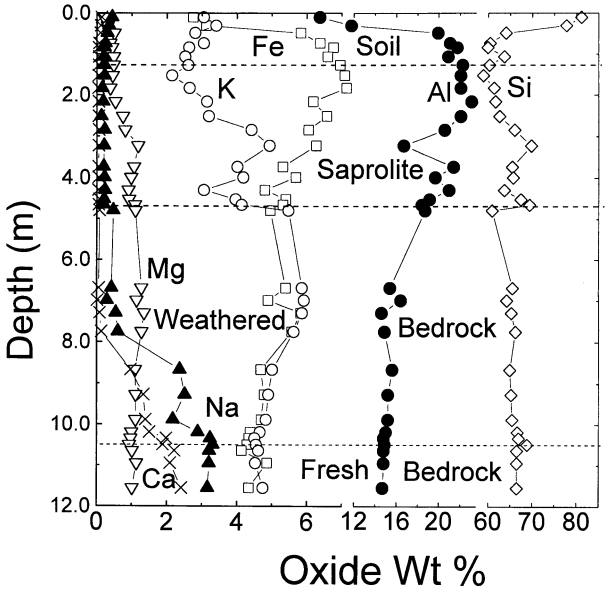

Fig. 3. Elemental distributions with depth in the Panola regolith.

The major secondary mineral in the regolith is kaolinite with lesser amounts of halloysite, goethite, hematite, gibbsite, and poorly ordered Fe-hydroxides (Schroeder and Melear, 1999). Electron backscatter images (EBS), coupled with energy dispersive X-ray analyses (EDAX), reveal that kaolinization of plagioclase is pervasive throughout the upper 10 m of the Panola regolith. The EDS photo in Figure 4A shows the initial stages of kaolinization of plagioclase at a 9.1 m depth in the Panola bedrock. Near-complete replacement of plagioclase was observed at a shallower depth of 7.5 m in the bedrock (Fig. 4B). Kaolinization is most commonly initiated within the grain cores, whereas residual remnants of plagioclase persist at grain boundaries. K-feldspar is essentially pristine in the weathered bedrock (Fig. 4A and 4B). K-feldspar weathering is initiated at the rock-saprolite interface (4.5 m). In the overlying saprolite, K-feldspar is extensively weathered as shown by the presence of kaolinite and open voids at depths of 2.8 and 1.8 m (Fig. 4C,D).

Element mobilities in the regolith result from the dissolution

Table 2. Elemental mobility (mol m^{-3}) and % loss from depth intervals (m) in the Panola regolith.

Depth	Bedrock 4.5–10.5	Saprolite 4.5–1.2	Soil 1.2–0.0	% loss
Si	**14,290**	−5,520	−160	16.5
Na	**8,190**	670	−90	73.8
Ca	**4,480**	40	−14	84.4
K	−450	**3,360**	120	18.5
Mg	100	**629**	−20	17.3
Fe	106	−120	**540**	−5.8
Al	1,652	−2,030	**1,780**	−1.0

Bold emphasizes progressive losses from different weathering environments.

Table 3. Mineralogy and compositions of Panola bedrock, saprolite, and soils.

Mineral	Formula	Quartz diorite[b]	Quartz diorite (11.5 m)	Quartz diorite (7.0 m)	Saprolite (4.8 m)	Saprolite (2.5 m)	Soil B Horz. (1.0 m)	Soil Horz. (0.1 m)
Quartz	SiO_2[a]	27.5	28.7	32.5	32.5	38.9	35.8	58.7
Plagioclase	$Na_{0.77}\ Ca_{0.23}\ Al_{1.23}\ Si_{2.77}\ O_8$	31.9	31.4	3.3	5.5	1.1	2.3	3.8
K-feldspar	$Na_{0.03}\ K_{0.97}\ Al_{1.02}\ Si_{2.99}\ O_8$	20.6	20.0	26.6	24.6	14.1	11.6	16.2
Biotite (rock)	$K_{2.00}(Mg_{1.78}\ Fe(II)_{3.05}\ Al_{0.51}\ Ti_{0.30})(Al_{2.40}Si_{5.60})O_{20}(OH)_4$	12.8	13.2	15.6	9.9	12.1	3.1	2.2
Muscovite	$K_{1.62}(Mg_{0.28}\ Fe(II)_{0.44}Al_{1.04}Ti_{0.10})(Al_{2.94}Si_{5.06})O_{20}(OH)_4$	7.2	6.7	6.7	6.7	6.7	6.7	6.7
Kaolinite	$Al_2Si2O^{10}(OH)_4$[a]	na	0.0	13.6	18.9	23.9	34.2	9.9
Fe oxides	FeO(OH)[a]	na	0.0	1.7	1.9	3.2	6.3	2.5

[a] Assumed compositions; na = not appliable.
[b] Average analyses by point count, communication from William Kelly, NY state Geologic Survey.

of primary silicate minerals and precipitation of secondary clays and oxides. Sequential calculations distribute these elements into residual phases based on mineral stoichiometry (Table 3). The mass of weathered plagioclase is first calculated on the basis of plagioclase stoichiometry, the fresh bedrock Na concentration and τ_{Na} values in the regolith. The residual Ca, Al, and Si remaining after distribution into the plagioclase are then calculated. Next, all of the initial Mg is partitioned into the

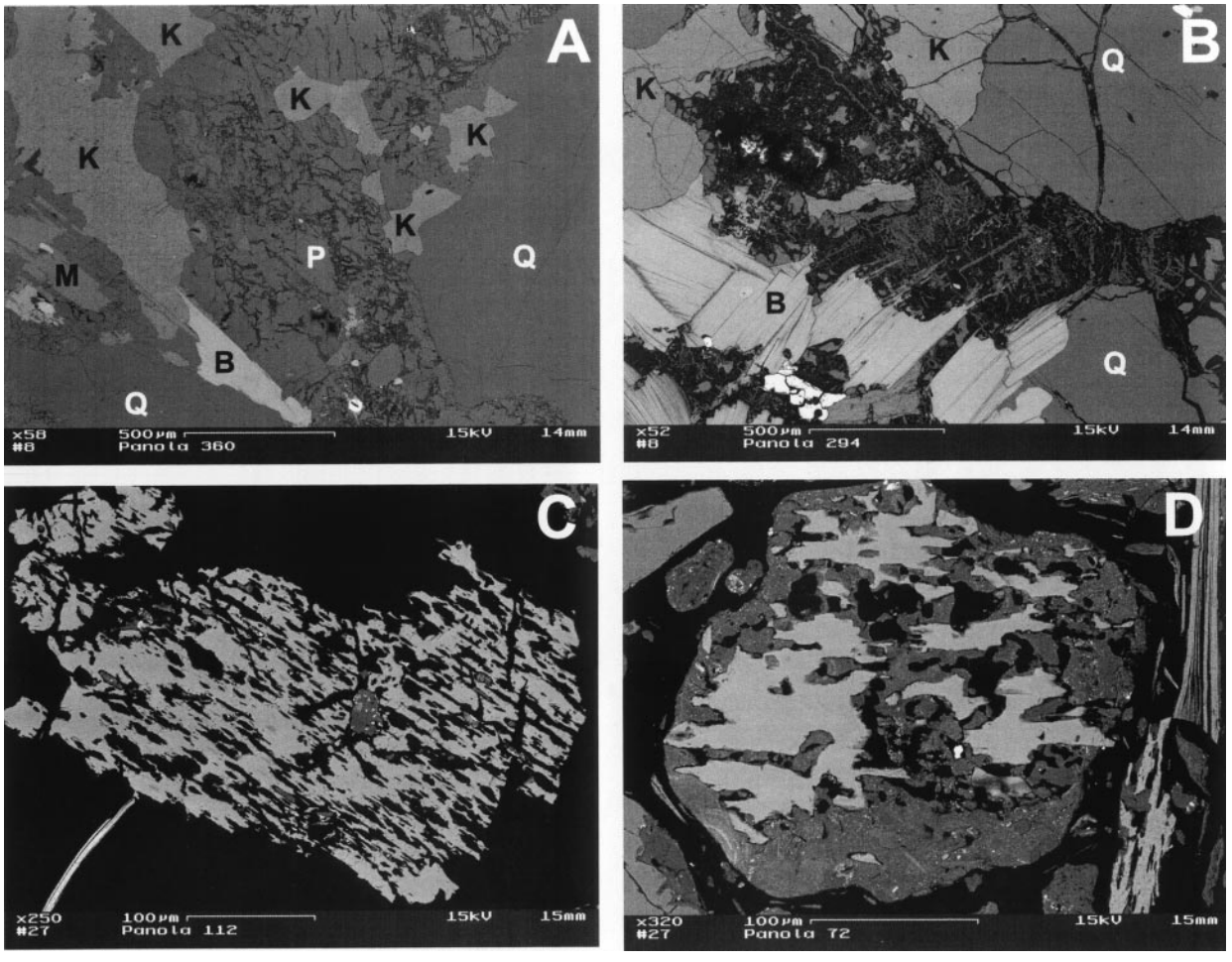

Fig. 4. SEM backscatter electron photomicrographs of thin sections from various depths in Panola regolith (*P* = plagioclase; K = K-feldspar; B = biotite; M = muscovite; and Q = quartz. (A) Initial plagioclase weathering at 9.1 m in the bedrock. Dark (clay filled) areas within the grain are kaolinite. Note the pristine nature of coexisting K-feldspar. (B) Plagioclase grains at 7.5 m depth. Plagioclase is virtually gone, leaving clay-filled vugs (black areas). The adjacent biotite is starting to weather along cleavage planes (dark areas within the biotite). The K-feldspar is pristine. (C) Saprolite from 2.8 m depth. The K-feldspar grain has dissolved, gaining a skeletal appearance with open vugs (black areas) that originally may have been partially filled with clay. (D) Saprolite from 1.8 m depth (just below soil-saprolite interface). The K-feldspar grain is partially replaced with clay. Note the relatively unreacted muscovite in the right of the image.

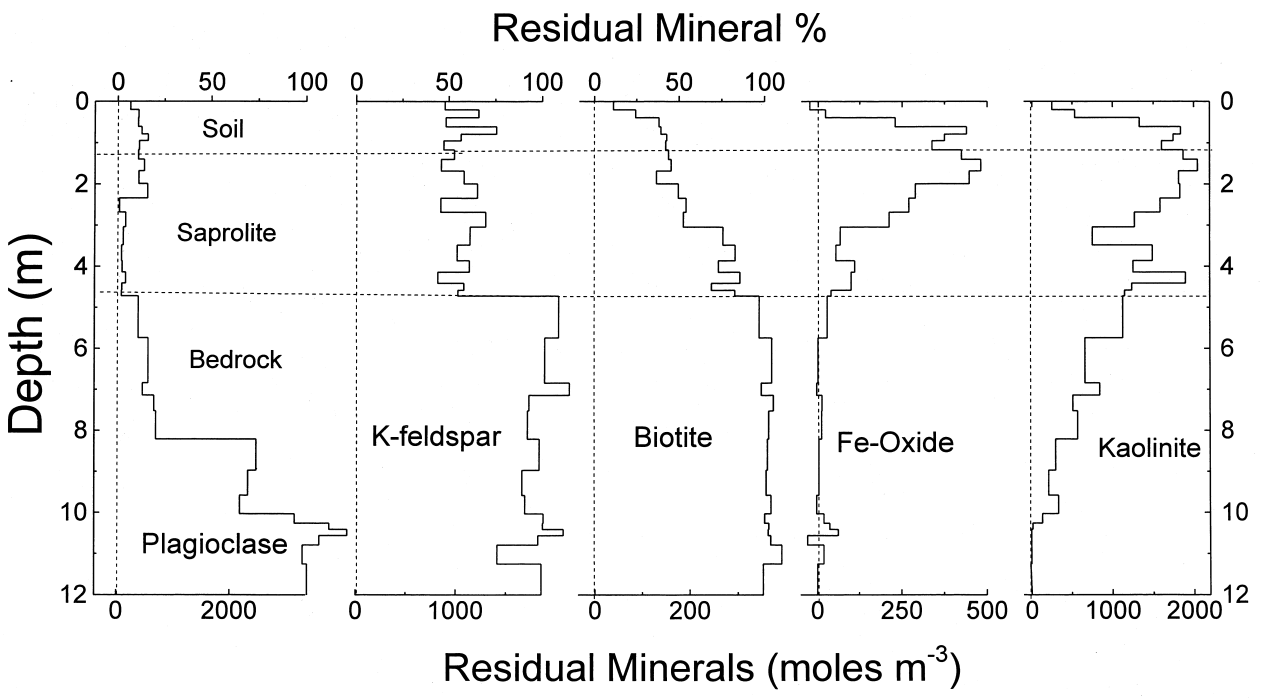

Fig. 5. Residual mineral distributions with depth in the Panola regolith. The lower horizontal axis is molar density, and the upper horizontal axis is the percentage of primary minerals remaining relative to the fresh granodiorite.

mica phases. It is not possible to distinguish between muscovite and biotite in the calculations because each mica contains the same set of elements, i.e., K, Mg, Fe, Ti, Si, and Al, although at different concentrations. Based on petrographic and chemical evidence for the nonreactivity of muscovite relative to biotite (see discussion of mica reactivities by White et al., 2001), the mass of muscovite was assumed to be constant as a function of depth and equal to that in the fresh bedrock (Table 3). All of the Mg is partitioned into biotite. The remaining steps sequentially distribute the residual K into the K-feldspar phase, the remaining Al into the kaolinite phase, the remaining Fe into Fe-oxide, and the residual Si into quartz. Hornblende was not considered in the above calculations because of low abundances (<2 wt.%). The close agreement between the calculated mineral distributions and the average modal analyses of the fresh granodiorite, as determined by point counting, validates the above procedure (Table 3).

Residual mineral abundances (mol m^{-3}), along with mineral percentages relative to their initial concentration in the unweathered granodiorite, are plotted in Figure 5. Initial bedrock weathering between 4.5 and 10.5 m removes 95% of the plagioclase from the fresh granodiorite. Petrographic observations show that this weathering corresponds to the extensive replacement of plagioclase by kaolinite (Fig. 4,B). In contrast, the proportion of K feldspar and biotite weathering out of the bedrock is essentially zero (Table 4), which correlates with the petrographic evidence showing the generally pristine nature of K-feldspar and biotite within the weathered bedrock (Fig. 4A,B). K-feldspar weathering is initiated abruptly at the saprolite-bedrock interface (Fig. 5) at which point ≈40% of the original K-feldspar is lost from the regolith. Residual K-feldspar in the overlying saprolite and soil horizons decreases modestly. The significant variability in K-feldspar contents are attributable to artifacts in the mass balance calculations that must first distribute K into the muscovite and biotite phases before the mass of residual K-feldspar can be calculated. The portion of biotite weathered at the saprolite-bedrock interface (15%) is much less than that for K-feldspar. However, the weathering and volumetric expansion of biotite is cited as the principal cause of the physical decomposition of the Panola Granite at the rock-saprolite boundary (Van Tassel and Grant, 1980). Residual biotite continues to weather out at progressively shallower depths in the saprolite and soil (Fig. 5) as discussed in greater detail by White et al. (2001).

The largest increase in kaolinite occurs within the bedrock because of the predominance of plagioclase weathering (Table 4 and Fig. 5). Al is not mobile in the bedrock, indicating that the conversion of plagioclase to kaolinite is conservative with respect to Al (Fig. 2C). The loss of kaolinite in the shallowest soils implies translocation and dissolution and reprecipitation in the underlying saprolite. Fe-oxides are formed by oxidation

Table 4. Mineral gains and losses (mol m^{-3}) in different weathering regimens and total % lost.

	Bedrock	Saprolite	Soil	% loss
Plagioclase	**−10,360**	1,690	−190	77.5
K-feldspar	−520	**−5,870**	−440	19.9
Biotite	126	**−2,330**	−87	19.0
Feoxides	41	460	**−260**	na[a]
Kaolinite	5,840	548	**−1,046**	na

Bold emphasizes progressive nature of weathering.
[a] na = not applicable.

Table 5. Average Sr concentrations and isotopic ratios in fresh Panola granodiorite and associated minerals.

	Sr (ppm)	$^{87}Sr/^{86}Sr$	$^{87}Rb/^{86}Sr$
Whole rock	nd[a]	0.7140	1.1163
Plagioclase	750	0.7083	0.0565
K-feldspar	600	0.7160	1.6088
Biotite	11	1.1060	8.1317
Muscovite	55	0.7548	9.4951
Hornblende	21	0.7098	0.3731

[a] nd = not determined.

of Fe released from biotite weathering in the saprolite (Fig. 5). Because of the stability of biotite, the amount of Fe-oxide produced in the underlying bedrock is low (Table 4). As in the case for kaolinite, Fe-oxides decrease in the overlying soils (Fig. 5). Positive τ_{Fe} values in the upper saprolite (Fig. 2C) suggest that Fe-oxides are partly derived from remobilization from the overlying soil.

3.4. Sr and $^{87}Sr/^{86}Sr$ Distributions

Sr concentrations and $^{87}Sr/^{86}Sr$ ratios for the bulk regolith are tabulated in Table 1 and for individual primary mineral phases in Table 5. As indicated, the elemental Sr concentrations are comparable in plagioclase and K-feldspar and are much lower in biotite and muscovite. $^{87}Sr/^{86}Sr$ ratios vary between 0.71406 and 0.72117 in the bulk regolith (Table 1). $^{87}Sr/^{86}Sr$ ratios are lowest in plagioclase and highest in the biotite (Table 5).

Elemental Sr and $^{87}Sr/^{86}Sr$ ratios are commonly used as surrogates for Ca mobility in chemical weathering studies (Graustein and Armstrong, 1983). However, in the Panola regolith, the mobility of Sr is very different from that of Ca (Fig. 6A). Although Ca is almost totally depleted, ($\tau_{Ca} \rightarrow -1$), significant Sr remains in the upper weathered bedrock, saprolite, and soil. This difference is related to the distributions of Ca and Sr in the feldspar phases. Calcium is contained only in plagioclase, whereas similar amounts of Sr are contained in plagioclase and K-feldspar (Table 5). Although it is commonly assumed that Sr follows Ca into plagioclase during initial stages of magma crystallization, the partition coefficients for Sr in K-feldspar are comparable with that for plagioclase (Arth, 1976); therefore, K-feldspar can effectively incorporate significant Sr if sufficient Sr remains in the magma during later stage crystallization. The difference in Sr and Ca mobilities in the Panola regolith correlates with very different weathering characteristics of plagioclase and K-feldspar. Concurrent biotite weathering does not significantly affect residual Sr distributions because of a low Sr content.

$^{87}Sr/^{86}Sr$ ratios of the bulk regolith are plotted vs. depth in Figure 6B. The ratios increase upward in the lower weathered bedrock but do not exhibit any significant trends in the overlying saprolite and soil. Measured $^{87}Sr/^{86}Sr$ values in the weathered regolith are compared with the expected ratios in Figure 6B (solid line) based on portions of residual minerals present and their respective Sr contents and $^{87}Sr/^{86}Sr$ ratios (Tables 3 and 5). Agreement is good between calculated and measured increases in $^{87}Sr/^{86}Sr$ in the bedrock where weathering is dominated by progressive plagioclase weathering. However, the measured $^{87}Sr/^{86}Sr$ ratios are relatively constant and lower than expected in the saprolite and soils. $^{87}Sr/^{86}Sr$ ratios should reach a maximum at the bedrock-saprolite interface due to depletion of K-feldspar and enrichment by residual radiogenic biotite. In the overlying saprolite, the calculated $^{87}Sr/^{86}Sr$ ratios decrease with the onset of biotite weathering. This is contrasted to the relative stability of the residual K-feldspar (Fig. 6B). This discrepancy is related to the fact that up to 50% of total Sr in the bulk saprolite and soil occurs as exchangeable Sr (1 N ammonium acetate) that does not reflect the residual mineral compositions.

Sources responsible for Sr mobilization can be determined graphically when the residual regolith $^{87}Sr/^{86}Sr$ ratios are plotted against the inverse ratio of Nb/Sr (Bullen et al. 1999). Nb behaves conservatively during weathering in the Panola rego-

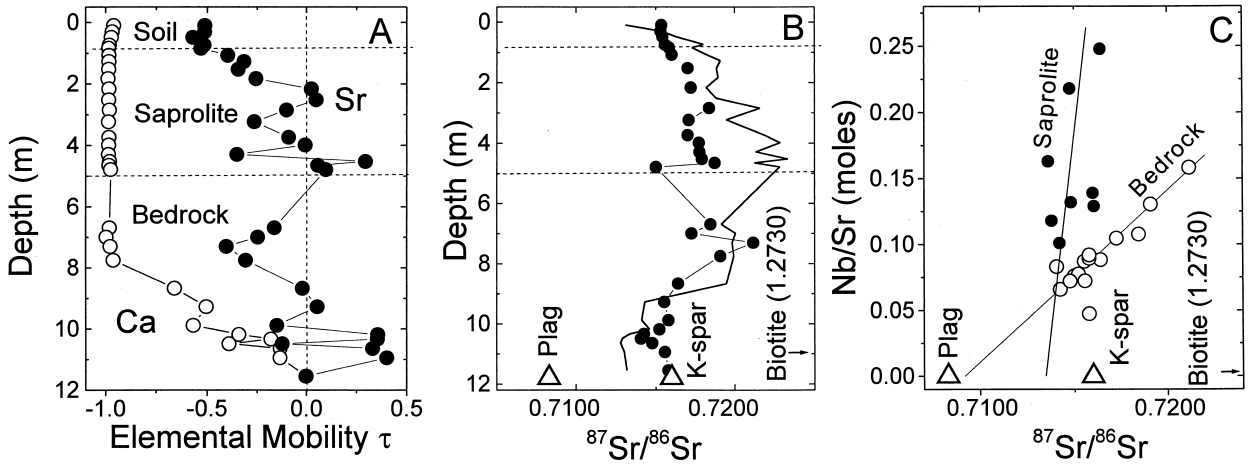

Fig. 6. Ca and Sr and $^{87}Sr/^{86}Sr$ variations with regolith depth. (A) Comparison of Sr and Ca mobilities in regolith. $\tau_{Ca,\,Sr} = 0$ signifies no mobilizations and $\tau_{Ca,\,Sr} = -1$ signifies complete mobilization. (B) Comparison of measured (open circles) and calculated (solid line) $^{87}Sr/^{86}Sr$ distributions with depth. Included are mineral isotopic compositions (triangles) used in mass balance calculations. (C) $^{87}Sr/^{86}Sr$ trends as functions of Nb/Sr ratios. Open circles correspond to bedrock ratios and closed circles to saprolite ratios.

Table 6. Representative chemical concentrations (μM) in soil-saprolite pore waters and ground water in Panola Watershed.

	Ridge top[a]					Upper hill slope[a]		Lower hill slope[a]		Ground water[b]
Depth (m)	0.3	0.91	1.83	3.00	4.62	0.3	1.2	0.3	1.27	2.5
pH	5.80	5.54	5.39	5.37	5.58	6.78	5.19	6.12	5.67	6.48
Na	24.3	40.0	202	206	163	32.9	35.6	31.0	67.0	117.2
K	41.0	36.2	43.7	17.7	12.9	49.1	7.6	16.2	46.3	14.5
Ca	55.9	25.5	24.1	12.5	14.5	129.1	42.4	99.3	29.6	17.2
Mg	30.4	81.7	66.5	56.4	35.2	51.7	13.5	57.4	36.5	19.0
Al	4.6	4.0	0.9	2.3	4.7	3.2	10.2	2.2	1.2	3.4
SiO_2	75.1	92.9	201	189	372	125	76.0	124	131	182.2
Cl	27.6	34.1	251	319	174	14.9	19.7	28.5	37.8	67.3
NO_3	1.4	1.1	23.8	2.8	2.1	1.4	1.4	1.4	0.7	0.7
SO_4	47.9	43.9	10.3	1.6	6.1	112	75.3	129	84.9	36.5
Alk (μEq)	86.9	63.4	30.8	25.4	55.6	133	12.0	20.6	9.7	59.4

[a] Sampled 1/21/93.
[b] Well 801, sampled 1/7/93.

lith (Fig. 2A), and the aqueous Nb/Sr ratio is expected to approach zero. In contrast, the Nb content of residual regolith will increase in the opposite direction from the origin, along a straight line, which defines the concurrent change in $^{87}Sr/^{86}Sr$ (Fig. 6C). The weathered bedrock data clearly plot along a trend that intersects the plagioclase isotopic composition. This coincidence shows that the $^{87}Sr/^{86}Sr$ variability in the bedrock is directly related to the amount of Sr mobilized during plagioclase weathering. Saprolite $^{87}Sr/^{86}Sr$ ratios plot along another trend distinctly different from that of the bedrock (Fig. 6C). The intersect denotes that the source component is more radiogenic than that of plagioclase (0.7083) and less radiogenic than K-feldspar (0.7160) but does not correspond to a specific mineral phase. This component may represent exchangeable Sr in addition to incongruent mineral weathering as shown for progressive changes in $^{87}Sr/^{86}Sr$ ratios for biotite (Bullen et al., 1997) and K-feldspar (Brantley et al., 1998) during natural and experimental weathering.

3.5. Water Compositions and the Thermodynamic Saturation of Feldspars

Representative pore water solutes obtained from the suction water samplers in the ridge soil and saprolite units are tabulated in Table 6. Also included were pore waters from the hill slope sites down gradient from the ridge top. Hydrologic saturation of pore waters in the Panola ridge top ranges from nearly 100% immediately above a fragipan at the soil-saprolite interface (1.6 m) to $<$50% in the lower saprolite. Based on hydrologic conductivity measurements, White et al. (2001) calculated a fluid residence time of 12 yr in the soil-saprolite. No water samples were obtained from the drill hole completed in granite at the ridge top site. However, representative groundwater compositions are included in Table 6, which were obtained from a well completed to a depth of 15 m in granite immediately down gradient from the lower gauge in the Panola watershed. Down hole information indicated flow was dominated by a saturated fracture intersected at a depth of 12 m. Pore and groundwater compositions and hydrology are discussed in greater detail by Burns (1998), Stonestrom et al. (1998), and White et al. (2001).

Rapid plagioclase weathering relative to K-feldspar in the Panola bedrock is in agreement with other natural weathering studies but contrasts with most experimental data that exhibit comparable dissolution rates at near-neutral pH values (Blum and Stillings, 1995). This discrepancy may be related to the fact that most experimental studies are short-term and conducted far from thermodynamic equilibrium. In contrast, natural weathering is long-term and mineral dissolution precedes much nearer thermodynamic saturation. Experimental evidence at elevated temperatures indicates that feldspar weathering rates decrease as solutions approach thermodynamic saturation (Burch et al., 1993; Oelkers et al., 1994).

The selective inhibition of feldspar weathering by thermodynamic saturation is not well established in regolith weathering studies. In reviewing the literature, White (1995) found that most soil pore waters were highly supersaturated with respect to both K-feldspar and plagioclase, in addition to the more soluble Al-hydroxide phases. Such supersaturation suggests that reported Al concentrations are excessive because of problems associated with sampling, filtration, and analyses, in addition to errors in calculating Al speciation. In the present study, regolith water compositions are speciated by using the PHREEQE-C code (Parkhurst, 1997). In addition to Al, mineral saturations are very sensitive to pH values, which were measured in pore waters degassed under vacuum in the porous cup water samplers. To more accurately reflect in situ pHs, the analyses were numerically re-equilibrated at 0.01 atm. CO_2, a partial pressure approximating that for soil gas influenced by plant respiration. CO_2 was not re-equilibrated for the groundwater samples.

Saturation indexes (SI), defined as the ratios of the ionic activity product over the solubility constant for the specified mineral (IAP/K_s), are plotted as functions of pH in Figure 7. Pore waters and groundwaters fall within the saturation range bracketed by amorphous $Al(OH)_3$ and crystalline gibbsite, which are both present in the Panola regolith (Schroeder and Melear, 1999). Soil and saprolite pore waters in the ridge top are significantly undersaturated with respect to albite (log SI = -7 to -3), a phase that approximates Na-rich oligioclase in the Panola granite (Fig. 7). Hill slope waters generally have a higher pH and are slightly closer to albite saturation. The hill slope soils, unlike the ridge top regolith, contain plagioclase in colluvium, which has eroded from ridge top granite outcrops

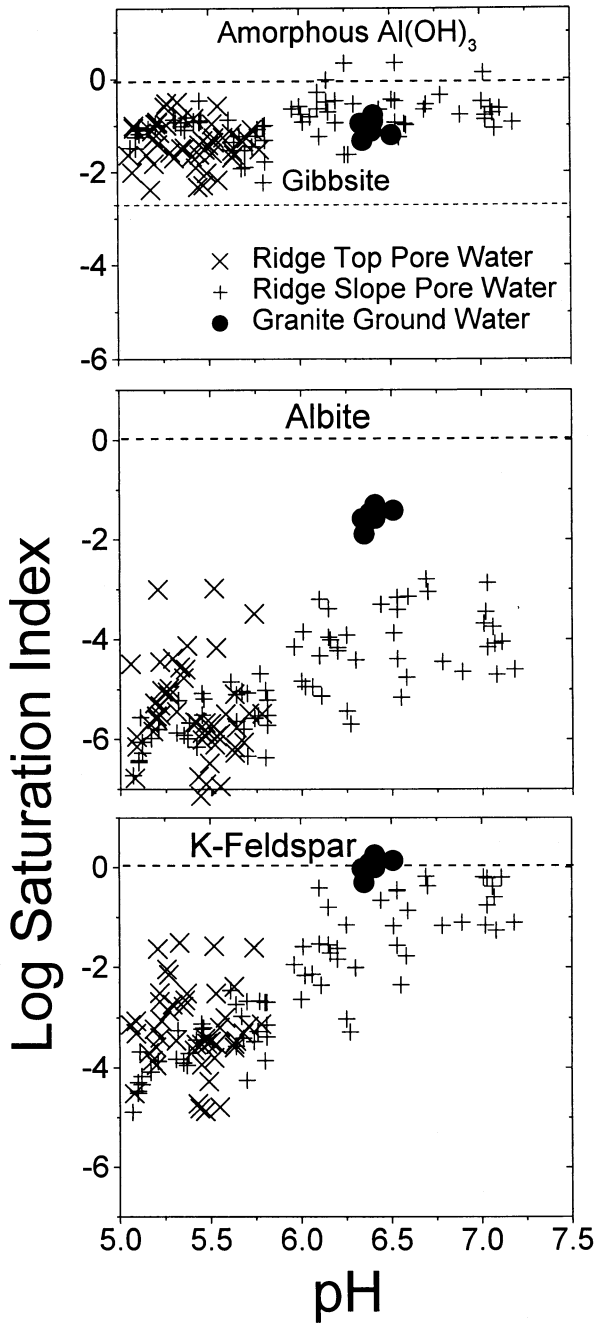

Fig. 7. Saturation indexes (SI = IAP/K_s) for regolith pore waters and ground waters with respect to (A) gibbsite, (B) albite, and (C) K-feldspar. Positive values correspond to thermodynamic supersaturation, and negative values correspond to undersaturation. SI values for crystalline gibbsite are calculated relative to amorphous $Al(OH)_3$.

(White et al., 2001). The groundwaters contained in granitic bedrock also are undersaturated with respect to albite (log SI = −1 to −2) despite abundant plagioclase in the fresh bedrock. Pore waters are much closer to K-feldspar saturation than albite (Fig. 7). A number of the hillslope pore waters are essentially saturated (log SI = 0). Most striking is the very close correlation between the groundwater compositions and calculated K-feldspar saturation. Such saturation explains the preservation of K-feldspar in the bedrock relative to the extensive weathering of plagioclase. Continued dissolution of plagioclase, which maintains elevated Al and Si concentrations in the groundwater, contribute, in part, to the thermodynamic stability of K-feldspar.

3.6. Comparison of Feldspar Weathering in Similar Granitic Regoliths

Numerous workers (Gardner, 1980; Calvert et al.; 1980; Buol and Weed, 1991; Cleaves, 1993 and Kretzschmar et al., 1997) have characterized the formation of other saprolitic regoliths derived from granitic rocks in the Piedmont Province of eastern United States. One particularly well-characterized weathering sequence is in the Davis Run watershed in the Piedmont Province in northern Virginia (Pavich, 1986; Pavich et al., 1989). The regolith in the upland area of the watershed consists of residual soil (1.5 m) overlying a thick saprolite (19 m) resting on granitic bedrock. Average mineralogy of the Occoquan Granite, described as an adamellite by Seiders et al. (1975), is quartz = 37%; K-feldspar = 27%; plagioclase An_6 = 21%; muscovite = 13%; and biotite = 2.1%. Using ^{10}Be concentrations, Pavich et al. (1995) calculated a minimum age of the Davis Run regolith surface to be 8×10^5 yr. On the basis of steady-state relationships between rates of erosion and saprolite formation, Pavich et al. (1995) calculated a saprolite propagation rate of 4 m myr^{-1}, which is in agreement with weathering rates based with loss of total dissolved solids from the Davis Run watershed (Pavich, 1986).

Elemental concentrations and bulk densities of the Davis Run regolith are presented in Table 7 (data from Pavich et al., 1989). Analogous to Panola, the volume calculation (Eqn. 2) assumes that Ti is immobile during weathering. Saprolite weathering is essentially isovolumetric, followed by a volumetric collapse in the overlying soil (Fig. 8A). The mobilities of Ca and Na, based on Eqn. 3, are very different in the Davis Run regolith compared with the Panola regolith (Figs. 2B and 8B). At Davis Run, Ca and Na persist in the thin sequence of weathered bedrock and in the saprolite immediately overlying it. Ca and Na progressively decrease to background levels with decreasing depth in the lower half of the thick saprolite. K behavior is also significantly different in the two regoliths. At Davis Run, no K decrease occurs at the saprolite-bedrock boundary. Rather, K decreases through the entire thickness of saprolite and soil (Fig. 8B).

The proportions of residual minerals present in the Davis Run regolith are calculated in a manner similar to Panola. All of the Na in Table 7 is apportioned into plagioclase based on the fresh Occoquan Granite composition and mineral stoichiometries reported by Seiders et al. (1975) and on τ_{Na} values (Fig. 8B). K occurs in both K-feldspar and micas in the Occoquan Granite. The mica is dominantly muscovite, which in the Panola study is shown to be highly unreactive compared with biotite (White et al., 2001). The lack of mica weathering in the Davis Run regolith is shown by the retention of Mg, except in the soil horizons. The loss of K in the Davis Run regolith is attributed principally to K-feldspar weathering.

Feldspar losses, expressed as percentages relative to the initial granite, are compared for the Panola and Davis Run regoliths in Figures 9 and 10. Both plagioclase and K-feldspar

Table 7. Horizons, depth, density, and compositions of the Davis Run Site (from Pavich et al., 1989).

	Depth (m)	Density (g cm^{-3})	SiO_2 (wt.%)	Al_2O_3 (wt.%)	Fe_2O_3 (wt.%)	MgO (wt.%)	CaO (wt.%)	Na_2O (wt.%)	K_2O (wt.%)	TiO_2 (wt.%)
Soil	0.60	1.54	67.0	16.5	4.60	0.50	0.08	0.30	1.90	1.10
	1.50	1.69	73.4	14.3	4.46	0.49	0.07	0.30	1.70	0.79
Saprolite	4.30	1.61	78.3	13.3	2.16	0.47	0.20	0.15	1.60	0.33
	6.70	1.51	70.9	17.3	2.06	0.49	0.03	0.07	2.50	0.34
	11.00	1.69	72.6	16.0	2.12	0.47	0.02	0.06	3.20	0.33
	15.00	2.00	79.3	12.7	1.50	0.37	0.36	0.84	2.60	0.26
	20.00	2.37	75.6	14.7	1.74	0.39	1.80	2.70	2.90	0.24
Weathered granite	21.00	2.52	74.7	15.2	1.86	0.40	2.20	2.80	3.20	0.25
Fresh granite	22.00	2.69	74.4	13.5	1.63	0.37	2.20	2.70	3.00	0.23

weathering are initiated immediately above the bedrock-saprolite interface at Davis Run. Feldspar losses increase linearly with decreasing regolith depth. Plagioclase is essentially 100% reacted at a depth of 12 m, whereas only 90% of the K-feldspar is reacted in the shallowest soil horizon. The contrasts between feldspar weathering in bedrock and saprolite environments at Panola and Davis Run are striking, considering similarities in rock type, regolith units, and topography. Regoliths developed on granites elsewhere in the Piedmont Province of southeastern United States, such as in North Carolina (Gardner, 1980) and South Carolina (Calvert et al., 1980), lack Ca and Na in the basal saprolite units, as is the case of Panola. However, more limited data suggest minimal Ca and Na losses in the underlying bedrock denoting a lack of plagioclase weathering.

4. DISCUSSION

An understanding of the differential rates of feldspar weathering requires quantification of the dynamic processes that affect specific reaction rates, solubility constraints, and hydrologic permeability in the natural weathering environment. Several previous studies have considered one or more of these parameters in terms of feldspar weathering in saprolite-laterite regoliths. Wang et al. (1995) and Nahon and Merino (1997) calculated mass balance distributions for the isovolumetric weathering of anorthite in tropical environments. The model proposed two coupled feldspar reactions. Pseudomorphic replacement of feldspar occurred under volume-constrained conditions at the rock-regolith interface, whereas congruent feldspar dissolution was assumed to occur directly above this replacement front. The model involved mass transport, specifically Al, on the microscopic scale of several grain diameters (<1 cm). This process, requiring extremely fast feldspar reaction rates, produced very sharp weathering fronts that are not typified by the Panola and Davis Run regoliths in which progressive feldspar weathering occurs over a scale of meters or tens of meters of regolith thickness (Figs. 2, 8, 9, 10).

Nesbitt et al. (1997) produced a reaction path model for the simulated weathering of Panola granite based on a regolith

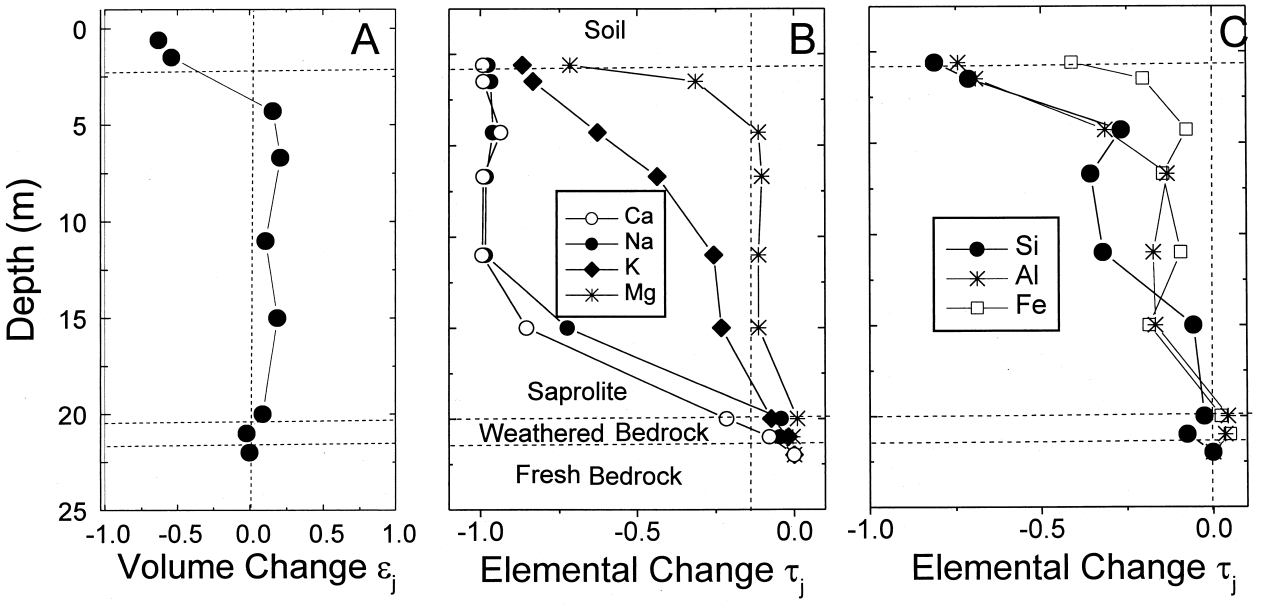

Fig. 8. Volume changes and elemental mass transfers within the Davis Run regolith. (A) Volumetric changes. Compaction and dilation are denoted by values of $\epsilon_i < 0$ and $\epsilon_i > 0$, respectively. A value of $\epsilon_i = 0$ denotes isovolumetric weathering. (B) Changes in Ca, Na, K, and Mg with regolith depth. (C) Changes in Si, Al, and Fe with regolith depth. A value $\tau_j = 0$ denotes no elemental loss, and a value of $\tau_j = -1$ denotes complete elemental loss.

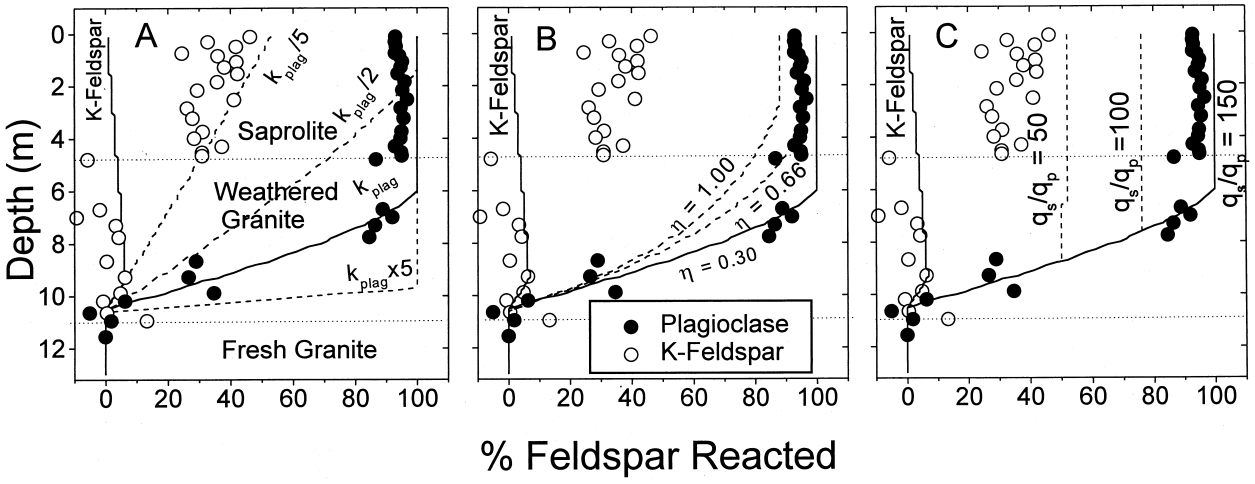

Fig. 9. Percent of feldspars reacted with depth in the Panola regolith. Solid and open circles are respective plagioclase and K-feldspar losses based on elemental mass balances. Solid lines are the best fits of the spreadsheet calculations for plagioclase loss with depth (Table 8). Dashed lines show the sensitivity of the calculations to changes in (A) the plagioclase rate constant, where $k_{plag} = 2.8 \times 10^{-16}$ mol m^{-2} s^{-1} (Eqn. 10), (B) the exponential volumetric surface area term, η (Eqn. 10), and (C) the ratio of the secondary to primary permeability q_s/q_p where $q_p = 7 \times 10^{-6}$ m yr^{-1}.

mineralogy presented by Grant (1963, 1975). Nesbitt assumed that the relative rate of plagioclase dissolution was 1.5 times faster than K-feldspar. An important result of the simulation was the rapid thermodynamic saturation of K-feldspar compared with the continued dissolution of plagioclase under thermodynamically undersaturated conditions. This model, however, did not specifically address the hydrologic implications involved in the observed differences in the weathering behavior of feldspars. To address this issue and to fit weathering rate constants to observed feldspar distributions in the Panola and Davis Run regoliths, a simple depth-time weathering model was developed by using an EXCEL spreadsheet.

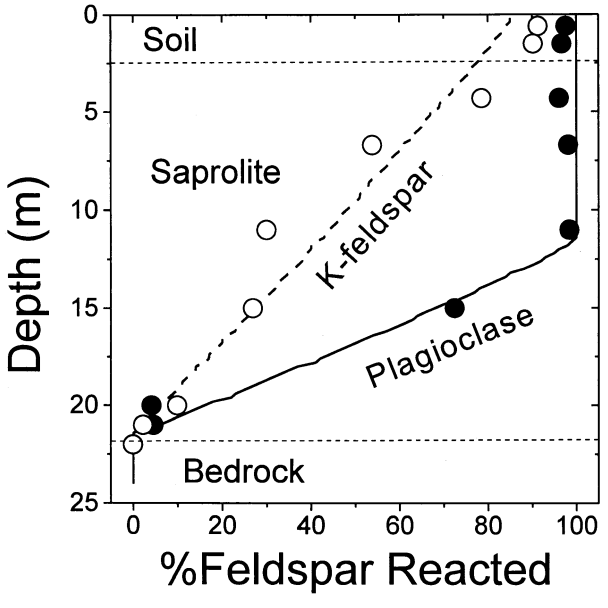

Fig. 10. Percent of feldspars reacted with depth in the Davis Run regolith. Solid and open circles are, respectively, plagioclase and K-feldspar losses based on elemental mass balances. Solid line and dashed lines are the best fits of the spreadsheet calculations to plagioclase and K-feldspar losses (Table 8) when $k_{plag} = 4.0 \times 10^{-17}$ mol m^{-2} s^{-1}, $k_{Kspar} = 1.5 \times 10^{-17}$ mol m^{-2} s^{-1}, $\eta = 0.20$ and $q_s/q_p = 800$.

Table 8 shows the initial portion of the spreadsheet used to produce the best fit to the observed plagioclase losses with depth in the Panola regolith (Fig. 9). For example, plagioclase loss R_t in cell H2 at depth d = 0.2 m and time t = 4000 yr (40 mol normalized unit Si) is the sum of the plagioclase reacted in that cell plus that reacted in R_{t-1} up to time step (t-1). The moles of feldspar weathered in cell H2 are calculated from a series of conditional statements that correspond to the proposed controls on feldspar weathering, i.e., permeability, residual mass, solubility, and reaction rates. The branching arrows in Table 8 point to the corresponding calculations based on these conditionalities. A second series of calculations defining K-feldspar reaction are run in a linked spreadsheet.

4.1. Primary and Secondary Hydraulic Conductivities

Feldspar weathering depends on the movement of reactants and products in the solvent phase. Within the fresh granite bedrock, the initiation of weathering is a function of the primary conductivity q_p (m yr^{-1}). This is considered by the first conditional statement in the spreadsheet calculation (Table 8). If for any given time step, the incremental depth is greater than the penetration depth of water, as determined by product of the primary hydraulic conductivity and total weathering time ($q_p \cdot t > d$), then the mass of the reacted feldspar is $R_i = 0$. This defines the condition of the pristine bedrock.

A critical assumption made in the calculations is that the weathering front advances at the rate at which meteoric water first penetrates into fresh granodiorite bedrock. A propagation rate of the weathering front of 7 m/10^6 yr at Panola (Bierman et al., 1995) translates into a primary conductivity of $q_p = 7 \times 10^{-6}$ m yr^{-1}. This value is more than an order of magnitude slower than the slowest hydraulic conductivity measured for fresh granites in laboratory and field studies (Table 9). These

Table 8. Sample section of spreadsheet used to calculate percentage of plagioclase weathered.

A	B	C	D	E	F	G	H	I	J	K	L	M	N
	Time =	0	1000	2000	3000	**t–1 = 3000**	**t = 4000**	5000	6000	7000	8000	9000	t→1.2 × 10^6
1	d = 0.10	0	0	20	20	20	40	40	40	40	60	60	736
2	**0.20**		0	0	20	**R_{t-1} = 20**	**R_t = 40**	40	40	40	60	60	736
3	0.30			0	0	20	40	40	40	40	60	60	736
4	0.40				0	0	20	40	40	40	60	60	736
5	0.50	**Permeability Control**				0	0	20	40	40	60	60	736
6	0.60	**IF(d>t_*q_p), no, yes → R_t = 0**						0	20	40	60	60	736
7	0.70	↓						0	0	0	20	40	736
8	0.80	**Mass Control**								0	0	20	736
9	0.90	**IF((k_{r*}((M_i-R_{t-1})/M_i))^e$_*$$S_v$ t)+R_{t-1})>M_i), no, yes → R_t = M_i**										0	736
10	1.00	↓										0	736
11	1.10	**Solubility control**										0	736
12	1.20	**IF(Log(0.0001+R_{t-1*}(2$_*$(R_{t-1}+R^1_{t-1})^2/(t_*q_{s*}1000)^3)+pH)>K_s), no, yes → R_t = $_{t-1}$**											
13	1.30	↓											
14	1.40	**Kinetic control**											
15	1.50	**R_t = R_{t-1}+k_{r*}((M_i-R_{t-1})/M_i))^n$_*$$S_{a*}$t**											
16	d→12.0	0	0	0	0	0	0	0	0	0	0	0	0

Fitted variables
q_s = secondary hydraulic conductivity = 1.7$_*$$10^{-6}$ m s^{-1}
e = surface/volume exponent = 0.30
k_r = reaction rate constant = 2.8*10^{-16} mol m^{-2} s^{-1}

Estimated independent variables
M_i = initial mass of plagioclase in depth interval = 830 mol
q_p = primary hydraluic conductivity = 8.6$_*$$10^{-6}$ m yr^{-1}
S_v = surface area per depth interval = 7.1 × 10^5 m^2 m^{-3}
K_s = log plagioclase solubility constant = −2.73
pH = 6.5

Rows correspond to increasing time (Δt = 1000 yr), and columns correspond to increasing depth (Δd = 0.1 m). R_t is the mass of plagioclase reacted (mol). Masses and rates are based on molar stiochiometries relative to unit silica.

conductivities are commonly measured for relatively rapid fluid movement along fractures in granite. Such fractures are evident in the Panola bedrock core and, undoubtedly, meteoric water has penetrated along them to depths significantly greater than the depth of the plagioclase weathering front (Fig. 9). However, the pervasive nature of plagioclase weathering in the granodiorite bedrock requires that slower fluid transport must also occur on a microscopic scale that involves the granite matrix (Fig. 2). On the basis of petrographic observations (Mosquera et al., 2000), primary matrix conductivity in granites is due to transgranular permeability associated with microfractures that cut across grain boundaries, intergranular permeability occurring along grain boundary contacts, and intragranular permeability associated with internal grain porosity.

Grain boundaries are commonly considered a principal avenue for matrix flow in crystalline rocks based on the documented importance of grain boundary diffusion for feldspars and other silicates at hydrothermal temperatures (Nagy and Giletti, 1986; Farver and Yund, 1993). However, on the basis of petrographic evidence in the present study, plagioclase weathering is initiated internally within the plagioclase grains and not at grain boundaries. As shown in Figure 4B, the plagioclase grain boundaries are often pristine and, in some instances, seem to be the last portion of the plagioclase grain to weather out. Internal weathering of plagioclase grains in granites was previously observed and was attributed to selective weathering of more calcic plagioclase cores (Clayton, 1986). However, based on microprobe data, such calcic zoning is not apparent in Panola plagioclases.

Plagioclase is considered the primary silicate phase with the

Table 9. Hydraulic conductivities in granite rocks and weathered regoliths (m yr^{-1}).

	Rock	Method	Reference
Primary granite conductivities q_p			
7 × 10^{-6}	**Fresh Panola Granite**	**Weathering rate**	**This paper**
6 × 10^{-6}	**Fresh Occoquan Granite**	**Weathering rate**	**This paper**
3 × 10^{-4} to 6 × 10^{-4}	Stripa Granite, Sweden	In situ, tracer	Abelin et al., 1991
3 × 10^{-4} to 3 × 10^{-1}	Bukit Timah Granite, Singapore	In situ, falling head	Zhao, 1998
6 × 10^{-4} to 2 × 10^{-2}	Beauvoir Granite, France	Core N_2 permeability	Galle, 1994
1 × 10^{-2} to 3 × 10^{0}	Granite, Illinois, USA	Core H_2O permeability	Morrow and Lockner, 1997
Secondary regolith conductivities q_s			
1 × 10^{-3}	**Weathered Panola Granite**	**Weathering rate**	**This paper**
>4.0 × 10^{-3}	**Davis Run Saprolite/Soil**	**Weathering rate**	**This paper**
3 × 10^{-2} to 1 × 10^{1}	Soil/Saprolite Panola, Georgia USA	Exp. sat. conductivity	Stonestrom et al., 1998
4 × 10^{-1} to 1 × 10^{2}	Soil/Saprolite, North Carolina USA	Exp. sat. conductivity	Schoeneberger et al., 1995
5 × 10^{-1} to 2 × 10^{0}	Saprolite, North Carolina USA	Exp. sat. conductivity	Vepraskas and Williams, 1995
3 × 10^{0}	Saprolite, Rio Icacos, PR	Exp. sat. conductivity	White et al., 1998

highest internal porosity in unweathered granite (0.5–1%; Montgomery and Brace, 1975). The extent to which this plagioclase porosity is interconnected within the granite fabric is critical to defining the primary conductivity of the granite. Plagioclase is one of the first major silicate phases to crystallize during magmatic cooling. Three-dimensional analyses of thin sections and X-ray-computed tomography have shown that during such cooling and subsequent settling, plagioclase forms chains of physically linked phenocrysts in granites and other crystalline rocks (Bryon et al., 1995; Philpotts, et al., 1999). In contrast, the latter nucleation and growth of other phenocrysts such as K-feldspar, are restricted to interstices of this crystalline framework and are thus more physically isolated. This interconnection of plagioclase phenocrysts, coupled with relatively high internal porosity, produces a network of conduits by which meteoric water first penetrates into the pristine granite matrix and initiates the type of pervasive internal plagioclase weathering observed at depth in the Panola granite.

Once the meteoric wetting front has reached a specific depth in the granite, chemical weathering commences. Initially, the weathering rate is expected to be extremely slow and limited by fluid conductivities approaching that of the primary granite. As proposed by Merino et al. (1993), the initial replacement of plagioclase by secondary minerals such as kaolinite may also be governed by volumetric constraints in which growth of the secondary phases produces stress-induced dissolution of the primary phase. Continued weathering produces mass losses that increase the granite permeability and, thus, the secondary hydraulic conductivity q_s. This process, under isovolumetric conditions, results in a continuing coupled feedback in which increasing permeability results in increased rates of weathering that produces further secondary permeability. The evolution of permeability in regoliths undergoing nonisovolumetric weathering, such as during volumetric collapse, is expected to be more complex.

4.2. Mass and Solubility Controls

If for any given time increment, the calculated weathering depth d is above the depth of the wetting front ($d \leq q_p \cdot t$), the calculation in Table 8 proceeds to the second conditional statement, which defines the limit on the total amount of plagioclase that can be reacted in the granite. This mass control compares R_t with the initial amount of plagioclase present M_i. Based on plagioclase compositions of the granite (Table 3) and estimated bulk densities, $M_i = 830$ mol for each depth interval ($\Delta d = 0.1$ m) in the fresh Panola. If the total mass reacted is equal to or greater than this initial amount of plagioclase, i.e., $R_t \geq M_i$, then R_t is reset to M_i.

If residual feldspar remains, i.e., $R_t < M_i$, the saturation index SI is then determined for plagioclase and K-feldspar. This is equivalent to comparing the ionic activity product IAP against K_s ($SI = IAP/K_s$), as is done by using the PHREEQE speciation code for Panola waters (Fig. 7).

Plagioclase and K-feldspar weathering are written in terms of the simplified alkali feldspar end members

$$NaAlSi_3O_8 + H^+ + 9/2\ H_2O \rightarrow Na^+ + 2H_4SiO_4 + 1/2\ Al_2Si_2O_5(OH)_4 \quad (5)$$

and

$$KAlSi_3O_8 + H^+ + 9/2\ H_2O \rightarrow K^+ + 2H_4SiO_4 + 1/2\ Al_2Si_2O_5(OH)_4 \quad (6)$$

where Al is fixed in the solid phase by the formation of kaolinite. Aqueous saturation is defined by the respective relationships (Parkhurst, 1997)

$$LOG\ (Na^+)(H_4SiO_4)^2 + pH = -2.73 \quad (7)$$

and

$$LOG\ (K^+) \cdot (H_4SiO_4)^2 + pH = -5.31 \quad (8)$$

where the Na, K, and Si activity terms are assumed equal to aqueous concentrations based on the dilute nature of the pore and ground waters (Table 6). The aqueous concentrations are determined both by the moles of feldspar reacted and the volume of solution that passes through a depth increment of regolith at a given time. The solubility of plagioclase is linked to the mass of reaction of K-feldspar reacted by the common concentration of dissolved silica. This explains the requirement for parallel calculations for plagioclase and K-feldspar weathering in the spreadsheets. These coupled calculations ignore the aqueous contribution of other silicates such as biotite.

Aqueous saturation for feldspar at time t can be established from the relationship (Table 8)

$$LOG((R_{t-1} \cdot (2(R_{t-1} + R'_{t-1}))^2/(t \cdot q_s \cdot 1000)^3 + pH = LOG\ K_s \quad (9)$$

where the left hand side of Eqn. 9 defines the ionic activity product IAP where R_{t-1} and R'_{t-1} are the masses of plagioclase and K-feldspar dissolved in the preceding time step (t-1) and q_s is the secondary hydraulic conductivity. The pH in Eqn. 9 is assumed to be 6.5 based on measurements for groundwater in the Panola granodiorite (Table 6). If at time step t in Table 8, the saturation index $SI = IAP/K_s > 1$, the reaction is stopped and R_t is set equal to R_{t-1}. Transition state theory, confirmed by experimental data for albite at elevated temperatures (Burch et al., 1993), predicts that feldspar dissolution rates diminish incrementally as undersaturated solutions approach thermodynamic saturation. The present calculations simplify this effect by assuming that weathering rates remain constant over the complete range of solution undersaturation, and reactions are terminated abruptly when saturation is achieved. The thermodynamic saturation state calculated by Eqn. 9 is also dependent on the fluid volume that has passed through a depth interval over time. This is determined as the product of time and the secondary hydraulic conductivity q_s (m yr^{-1}). In reality, permeability is expected to increase with the degree of isovolumetric weathering. However, in the calculations, it is represented by a single average secondary hydraulic conductivity q_s, which is used as a fitting parameter with the assumption that $q_s \geq q_p$.

4.3. Kinetic Controls

The system is kinetically limited only if the preceding criteria are met in the calculations: (1) the reaction occurs above the wetting front, which is spatially determined by the primary

hydraulic conductivity q_p and the reaction time; (2) residual feldspar remains to react, i.e., $R_t < M_i$; and (3) the solution composition based on feldspar reaction and secondary permeability q_s remains thermodynamically undersaturated, i.e., SI < 1. If these conditions are met, the mass of feldspar reacted R_t up to time t is then calculated from the rate expression (Table 8)

$$R_t = R_{t-1} + k_r((M_i - R_{t-1})/M_i)^{\eta} \cdot S_v \cdot t \quad (10)$$

where k_r (moles m^{-2} s^{-1}) is the reaction rate constant. The term $(M_i\text{-}R_{t-1})/M_i$ defines the mass of feldspar remaining. S_v (m^2m^{-3}) is the volumetric surface area, which is the total surface area of feldspar defined by unit depth d (m) and the horizontal surface (1 m^2), and η is the exponential function relating residual mineral mass to volumetric surface area.

The volumetric surface area S_v can be calculated from the specific feldspar surface area S (m^2 g^{-1}) from the relationship

$$S_v = (S \cdot A \cdot d \cdot 10^6)/\rho \quad (11)$$

where ρ is the rock density (2.65 g cm^{-3}). The specific surface areas for weathered feldspars in granites has not been measured but is estimated to be S = 1 m^2 g^{-1} based on average values reported for feldspars weathered over 6×10^5 yr in alluvial granitic sediments (White et al., 1996). Much of the increase in surface area with weathering observed in that study was attributed to internal surface areas of the mineral grains. This also appears to be the principal process by which surface areas are created during weathering of the Panola Granite, as evidenced by the microphotographs in Figures 4A and 4B.

The volumetric surface area at time t is related to the mass of residual feldspar present, i.e., $(M_i\text{-}R_{t-1})/M_i$ by the exponential term η in Eqn. 10. This relationship is not expected to be a direct proportionality i.e., $\eta \neq 1$ (Lasaga, 1984; White et al. 1996). For example, if feldspar crystals were simple spheres, the geometric relationship between surface and volume is $\Delta S \propto \Delta V^{2/3}$ ($\eta = 0.66$). Thus, during weathering, the surface area is expected to decrease at a rate that is exponentially slower than the decreases in volume and mass of the feldspar grains. Feldspar crystals are not geometric spheres. However, η is required to be less than unity to enable feldspar weathering to go to completion, i.e., $R_t \rightarrow M_i$ as $Sv \rightarrow 0$.

4.4. Fitting the Model to the Feldspar Weathering in the Panola Regolith

The spreadsheet calculations in Table 8 are fitted to the feldspar profiles in the Panola regolith (Fig. 9) based on the relationship that the percentages of plagioclase and K-feldspar reacted are equal to $100 \times R_i/M_i$. The best fit (solid lines) shows that no plagioclase is weathered below 10.5 m, a progressive increase in reacted plagioclase occurs between 10.5 and 6.5 m and that 100% of the plagioclase is depleted ($R_t \rightarrow M_i$) above 6.5 m. (Fig. 9, solid lines). A slightly smaller plagioclase loss based on elemental mass balances (95%) reflects limited retention of Na in the regolith, probably in the form of weathering-resistant minerals. At the same time, spreadsheet calculations show that K-feldspar remains essentially unreacted in the bedrock. The complex behavior of K-feldspar weathering at and above bedrock/saprolite interface is not considered in the spreadsheet calculations. Significant K-feldspar weathering may be related to groundwater that flows along the bedrock surface and is thermodynamically unsaturated with K-feldspar. Such thermodynamic undersaturation persists in the overlying saprolite (Fig. 7).

Variables fitted to feldspar weathering in the Panola bedrock are the kinetic rate constants for plagioclase and K-feldspar, k_{plag} and k_{Kspar}, the exponential surface area term η and the secondary hydraulic conductivity, q_s. The remaining terms tabulated in Table 8 are based on independent estimates discussed in the preceding sections. The modeled reactivity is quite sensitive to the kinetic rate constant for plagioclase. A value of $k_{plag} = 2.8 \times 10^{-16}$ mol m^{-2} s^{-1}, based on the plagioclase stoichiometry presented in Table 3, produces the best fit for plagioclase weathering (Fig. 9A, solid line). Increasing k_{plag} by a factor of 5 results in a very flat weathering profile in which plagioclase is completely removed over a very small depth interval immediately above the unweathered granite (Fig. 9A, dashed line). Decreasing k_{plag} by factors of 2 and 5 result in progressively steeper plagioclase profiles in which up to 50% of the plagioclase persists in the upper soil horizon.

The linear relationship between the vertical distribution of reacted feldspar (Fig. 9) and the kinetic rate constant k_{plag} can be independently validated by using a simple but useful graphical technique where

$$R_i = d/b_{plag} \quad (12)$$

where b_{plag} is the slope of the linear correlation between depth and plagioclase mass loss R_i ($b_{panola} = -1.5 \times 10^{-3}$ m/mol m^{-3}; $r^2 = 0.82$), and d is a specified depth in the regolith. The rate of mass loss with depth is inversely proportional to the slope of the data, i.e., the shallower the weathering trend with depth, the more rapid the rate of plagioclase weathering.

The rate of change in regolith thickness d, as the weathering front progresses downward through the regolith, is defined as w_{reg} (m s^{-1}) or approximately 7 m/10^6 yr based on ^{36}Cl data (Bierman et al., 1995). Substituting into Eqn. 12 produces a plagioclase weathering rate per unit volume of saprolite r_{plag} (mol m^3 yr^{-1}).

$$r_{plag} = w/b_{plag} \quad (13)$$

This rate r_{plag} is converted into the kinetic rate constant k_r (mol m^{-2} s^{-1}) by incorporating the volumetric surface area for plagioclase (Eqn. 11)

$$k_{plag} = w/(b_{plag} \cdot S_v) \quad (14)$$

In the spreadsheet approach, S_v is incrementally decreased as the mass of residual plagioclase is decreased (Eqn. 10). In the graphical approach (Eqn. 14), this is not possible, and S_v is taken to be the surface area of one half of the residual plagioclase (3.5×10^5 m^2m^{-3}).

The reaction rate constant based on the graphical approach (Eqn. 14) is $k_{plag} = 4.1 \times 10^{-16}$ mol m^{-2} s^{-1}, which is only slightly more than that calculated from the spread sheet approach, i.e., 2.8×10^{-16} mol m^{-2} s^{-1}. For regoliths in which a primary mineral exhibits a discernable distribution with depth due to weathering, the kinetic rate constant is tightly constrained if the propagation rate of the weathering front can be estimated. This is a characteristic of regolith weathering not commonly recognized nor used in the calculation of kinetic rate constants.

The exponential term η, which relates the surface area to the

mass of residual feldspar (Eqn. 10), is the second fitting parameter describing the distribution of feldspar reacted in the Panola Granite. Increasing the value of η produces progressively stronger curvatures to the fits of the data in which mass of reacted plagioclase asymptotically decreases with decreasing depth (Fig. 9B). A value of $\eta = 0.66$ assumes a spherical geometric relationship between surface area and volume (mass) of residual plagioclase. A value of $\eta = 1.00$ assumes a direct relationship between the amount of residual feldspar present and its corresponding surface area. If half the mass is reacted, then half the surface area remains. The plagioclase is never completely consumed at these high η values because the decrease in reaction rate becomes directly proportional to the decrease in the volumetric surface area S_v (Eqn. 10). The best fits to the data, using values of $\eta \leq 0.30$, produce nearly linear inverse correlations between the percentages of plagioclase reacted and depth (Fig. 9B). Low values for η imply a low correlation between the mass of plagioclase weathered and the volumetric area S_v. This requires a significant increase in the specific surface S of the feldspar during weathering (Eqn. 11). This increase corresponds to the development of roughness and internal porosity observed within weathered plagioclase grains in the granitic bedrock (Fig. 4).

The secondary hydraulic conductivity q_s is the final fitting parameter in the spreadsheet calculations (Fig. 9C). The value for q_s fixes the pore water volume that passes through the weathered granite for each time increment. This volume, coupled with the mass of reacted mineral, determines the thermodynamic saturation state of the feldspars (Eqn. 9). The secondary conductivity q_s can be expressed as a ratio relative to the primary conductivity, which is independently estimated on the basis of assumed steady-state weathering and cosmogenic age dating of the regolith ($q_p = 8.6 \times 10^{-6}$ m yr^{-1}). The best fit to the plagioclase data in Figure 9C is produced when the secondary conductivity is significantly larger than the primary conductivity, i.e., $q_s/q_p = 150$ ($q_s = 1.3 \times 10^{-3}$ m yr^{-1}). This ratio ensures that plagioclase does not reach thermodynamic saturation in the bedrock but rather continues to react until its mass is exhausted at a depth of 6.5 m ($R_t = M_i$). The magnitude of the calculated difference between q_p and q_s is in accord with the two to four orders of magnitude increase in permeabilities of weathered granites compared with fresh granites (Beavis, 1985). If the secondary conductivity is decreased, as shown by the ratios $q_s/q_p = 100$ and $q_s/q_p = 50$ (Fig. 9C), plagioclase becomes thermodynamically saturated at lower and lower amounts of reacted feldspar (Fig. 9C, dashed vertical line segments).

The extent of K-feldspar reaction, compared with plagioclase, is controlled both by the relative reaction rates and the saturation states of the two feldspars. The best fit of the kinetic rate constant for K-feldspar $k_{Kspar} = 9.5 \times 10^{-17}$ mol m^{-2} yr^{-1} based on the stoichiometry presented in Table 3, produces very limited K-feldspar reaction, which is in accord with the observed stability of K-feldspar in the weathered Panola Granite (Figs. 4A,B). A ratio of $k_{plag}/k_{Kspar} = 3.4$ produces the best fit to the relative proportions of plagioclase and K-feldspar reacted at a specific weathering depth (Fig. 11). This ratio is consistent with experimental data, indicating that plagioclase dissolution rates are only slightly faster than K-feldspar far from equilibrium and at neutral pHs (Table 10).

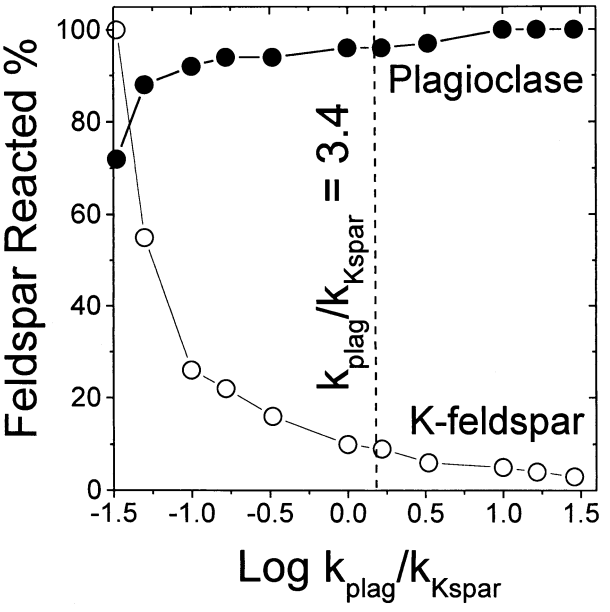

Fig. 11. Calculated percent of plagioclase (solid circles) and K-feldspar (open circles) reacted as a function of the ratio of the K-feldspar to plagioclase rate constants at a depth of 6.5 m in the Panola bedrock. The vertical dashed line is the best fit of k_{Kspar}/k_{plag} to the feldspar data presented in Figures 9 and 10 for the regoliths.

The calculations, however, are not particularly sensitive to the values used for the K-feldspar rate. As shown in Figure 11, the K-feldspar rate must be 10 times greater than for plagioclase, i.e., $k_{plag}/k_{Kspar} = 0.1$, for significant amounts of K-feldspar to weather in the granitic bedrock (Fig. 11). Such rapid K-feldspar rates are not in accord with the relative feldspar rates determined in experiment and natural studies. The selectivity of plagioclase relative to K-feldspar weathering in the bedrock is more strongly dependent on their respective solubilities than on their kinetic rate constants. Albite, the end member Na-plagioclase, is approximately 400 times more soluble than is K-feldspar (Eqn. 7 and 8). Weathering selectivity is, therefore, very sensitive to the hydrologic regimen, which controls fluid volumes, and, therefore, thermodynamic saturation. This is shown in Figure 12A where plagioclase and K-feldspar reactivities at a specific depth in the weathered Panola bedrock are plotted against ratios of the secondary to primary hydraulic conductivities. When secondary conductivities approach that of the fresh granite log $q_s/q_p < 1$), both plagioclase and K-feldspar reactivities are strongly suppressed by thermodynamic saturation (Fig. 12A). Plagioclase reactivity sharply increases in the range log $q_s/q_p = 1$–2, which is the transition from saturation-suppressed to kinetically controlled reaction. Plagioclase becomes totally reacted, i.e., $R_t = M_i$ (Table 8), at a conductivity ratio $q_s/q_p = 150$.

Within the conductivity range (log $q_s/q_p = 1$–2), K-feldspar reactivity remains strongly suppressed due to thermodynamic saturation (Fig. 12A). This saturation is produced both by the initial stages of K-feldspar dissolution in addition to significant amounts of silica contributed from the more soluble plagioclase (Eqn. 5 and 6). At log $q_s/q_p > 2$, K-feldspar becomes undersaturated, and the reactivity increases upward to 60% at a log

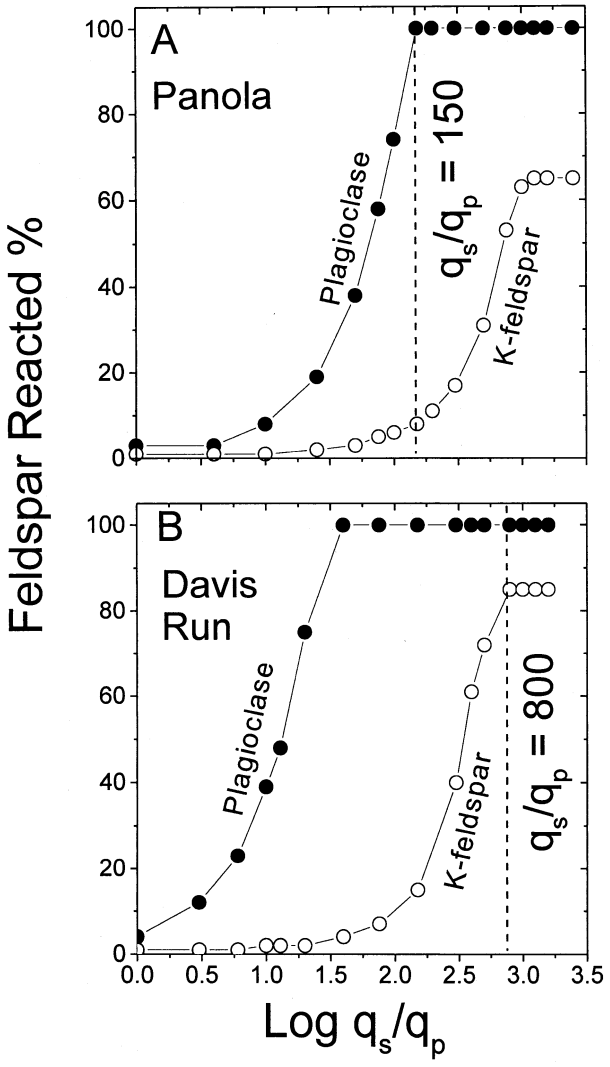

Fig. 12. Calculated percent of plagioclase (solid circles) and K-feldspar (open circles) reacted as function of the ratio in secondary to primary hydraulic conductivities. Reactions at (A) 6.5 m depth in the Panola regolith and (B) 0.2 m depth in the Davis Run regolith. Vertical dashed lines are the best fits of q_s/q_p to the feldspar data presented in Figures 9 and 10.

$q_s/q_p = 3$. K-feldspar is completely controlled by kinetic reaction at higher q_s/q_p ratios. For the fitted rate constant, $k_{Kspar} = 9.5 \times 10^{-17}$ mol $m^{-2}s^{-1}$, K-feldspar is not completely consumed at the maximum reaction time, i.e., $R_t < M_i$.

4.5. Fitting the Model to the Feldspar Weathering in the Davis Run Regolith

Plagioclase and K-feldspar are both stable within the Occoquan Granite at Davis Run below the saprolite-bedrock interface (Fig. 10). This implies that, unlike the Panola Granite, insignificant volumes of fluid have penetrated into the bedrock in advance of the saprolite weathering front. As in the case of Panola, the primary conductivity is assumed equivalent to the steady-state propagation rate of the weathering front, which is determined to be $q_p = 4 \times 10^{-6}$ m yr^{-1} based on cosmogenic age dating and watershed mass balances (Pavich et al., 1995). The initial masses in a 0.10-m depth interval of Occoquan Granite are $M_{plag} = 490$ mol and $M_{Kspar} = 327$ mol. The specific surface area for both plagioclase and feldspar is assumed to be equivalent to that of the Panola feldspars, $S = 1.0$ m^2 g^{-1}. The pH of the pore waters is also assumed to be comparable to pore water values measured in the Panola saprolite pH = 5.5 (Table 4).

The best fits to the percentages of plagioclase and K-feldspar weathered from the saprolite and soils overlying the Occoquan Granite are shown in Figure 10 (solid and dashed lines) using respective rate constants of $k_{plag} = 4.0 \times 10^{-17}$ mol $m^{-2}s^{-1}$ and $k_{Kspar} = 1.5 \times 10^{-17}$ mol $m^{-2}s^{-1}$. Plagioclase reacts 2.5 times faster than K-feldspar. A fitted value of $\eta = 0.20$ was used for the exponential term in the volumetric surface area relationship (Eqn. 10). As in the case of the Panola regolith, linearity between the percent of reacted feldspars and decreasing depths implies a low correlation between decreases in mineral mass and decreases in specific surface area. The linearity between mineral losses and regolith depth implies that both plagioclase and K-feldspar weathering are kinetically controlled and not inhibited by thermodynamic saturation with pore water in the Davis Run saprolite. The effect of changes in the ratios of secondary to primary conductivity q_s/q_p on solution saturation and percentages of reacted plagioclase and K-feldspar is shown in Figure 12B. At log $q_s/q_p < 1$, plagioclase reaction is strongly suppressed by thermodynamic saturation due to low fluid flow rates (Eqn. 9). Between log $q_s/q_p = 1$ and 2, as the flow rates increase, the plagioclase weathering accelerates, becoming kinetically controlled (Eqn. 10). Over this conductivity range, K-feldspar reaction continues to be suppressed due to solution saturation.

The situation at log $q_s/q_p = 1.5$ for the Davis Run regolith is equivalent to the best fit for the weathered Panola Granite in which all the plagioclase is reacted but almost all of the K-feldspar remains (Fig. 12A). At $q_s/q_p > 1.5$ the K-feldspar weathering accelerates, becoming increasingly controlled by kinetic reaction. The reaction becomes independent of the secondary conductivity at $q_s/q_p = 800$ at which point the reacted K-feldspar is equal to that calculated from mass balances (85%). This corresponds to a secondary conductivity of $q_s = 3.9 \times 10^{-3}$ m yr^{-1}. As shown in Figure 12B, increasing the q_s/q_p ratio in excess of 800 does not produce further increases in reacted K-feldspar because it is completely kinetically controlled and not dependent on the permeability. Increasing the value for k_{Kspar} would increase the percentage of K-feldspar reacted (Eqn. 1) but it would also decrease the goodness of the fit to the Davis Run regolith data (Fig. 10).

The preceding analysis indicates that the secondary conductivity q_s in the Davis Run regolith must exceed 3.9×10^{-3} m yr^{-1} for both plagioclase and K-feldspar dissolution to be kinetically controlled and not inhibited by thermodynamic saturation. Although no hydrologic information is available for the Davis Run regolith, this predicted q_s can be compared with experimentally measured conductivities for soil-saprolites for the Piedmont Province of the United States and elsewhere (Table 9). These values vary between 3×10^{-2} and 1×10^{2} m yr^{-1} for other soil-saprolites depending on the permeability and degree of hydraulic saturation. These values are at least an order of magnitude faster than the minimum calculated con-

Table 10. Comparison of natural and experimental dissolution rates of selected feldspars.

	Rate (log mol m^{-2} s^{-1})	pH	Surface area	Environment	Age[a] k yr	Reference
Plagioclase						
Albite	−11.0	6.0	BET	Experiment, crushed	na	Welch and Ullman, 1996
Albite	−11.1	5	BET	Experiment, crushed	na	Holdren and Seyer, 1985
Oligoclase	−11.4	5	BET	Experiment, crushed	na	Mast and Drever, 1987
Oligoclase	−11.6	5.4	BET	Experiment, crushed	na	Stillings et al., 1996
Oligoclase	−11.8	5.0	BET	Experiment, crushed	na	Busenberg and Clemency, 1976
Albite	−11.9	5.6	BET	Experiment, crushed	na	Chou and Wollast, 1985
Oligoclase	−12.0	5.0	BET	Experiment, crushed	na	Oxburgh et al., 1994
Oligoclase	−12.1	5.0	GEO	Trnavka River watershed, Czech.	10	Paces, 1986
Oligoclase	−11.8	nd	GEO	Plastic Lake, Ontario, Canada	10	Kirkwood and Nesbitt, 1991
Albite	−12.1	5.0	BET	Experiment, crushed	na	Knauss and Wolery, 1986
Oligoclase	−12.5	6.8	GEO	Coweeta Watershed, North Carolina, USA	nd	Velbel, 1985
Oligoclase	−13.1	5.6–6.1	BET	Gardsjon watershed soil, Sweden	10	Sverdrup, 1990
Oligoclase	−13.3	2.0–4.5	GEO	Bear Brook watershed soil, Maine, USA	10	Swoboda-Colberg and Drever, 1992
Labradorite	−13.7	6.0–7.5	GEO	Crrystal Lake aquifer, Wisconsin, USA	10	Kenoyer and Bowser, 1992
Oligoclase	−14.5	5.8	GEO	Bear brook Watershed, Maine, USA	10	Schnoor, 1990
Oligoclase	−14.5	5.0	BET	Experiment, weathered soil, California, USA	nd	Suarez and Wood, 1995
Andesine	−14.7	5.0	GEO	Filson Ck. Watershed, Minnesota, USA	10	Siegel and Pfannkuch, 1984
Oligoclase	**−15.7**	**6.5**	**BET**	**Panola bedrock, Georgia, USA**	**250–500**	**This study**
Oligoclase	−15.9	5.0–6.5	BET	Soil chronosequence, Merced, California, USA	10–3,000	White et al., 1996
Albite	**−16.4**	**nd**	**BET**	**Davis Run saprolite, Virginia, USA**	**>850**	**This study**
K-feldspar						
K-feldspar	−11.1	5.0	BET	Experiment, crushed	na	Holdren and Speyer, 1985
K-feldspar	−11.8	nd	GEO	Plastic Lake, Ontario, Canada	10	Kirkwood and Nesbitt, 1991
Orthoclase	−12.3	5.0	BET	Experiment, crushed	na	Busenberg and Clemency, 1976
Microcline	−12.8	5.6	BET	Experiment, crushed	na	Schweda, 1989
K-feldspar	−12.9	nd	BET	Shap Granite, natural etch pits	5	Lee et al., 1998
K-feldspar	−13.3	5.6–6.1	BET	Gardsjon watershed soil, Sweden	12	Sverdrup, 1990
K-feldspar	−13.3	4.5	GEO	Bear Brook watershed soil, Maine, USA	12	Swoboda-Colberg and Drever, 1992
K-feldspar	−14.2	5.0	BET	Experiment, weathered soil, California, USA	nd	Suarez and Wood, 1996
K-feldspar	−14.7	nd	GEO	Soil catena, Illinois, USA	12	Brantley et al., 1992
Anorthoclase	−16.5	5.0–6.5	BET	Soil chronosequence, Merced, California, USA	10–3,000	White et al., 1996
K-feldspar	**−16.8**	**nd**	**BET**	**Davis Run Saprolite, Virginia, USA**	**>850**	**This study**

[a] Age refers to the estimated duration of natural feldspar weathering.

ductivity required to maintain thermodynamic undersaturation in the Davis Run. This implies that kinetically controlled feldspar weathering is expected to be the norm in such high porosity and permeable saprolites.

4.6. Comparing Feldspar Weathering Rates

The reaction rate constants determined by the spreadsheet calculations for feldspar weathering in the Panola and Davis Run regoliths are compared in Table 10 with values reported in the literature for comparable feldspars reacting under experimental and natural conditions. Comparisons can be made both in terms of relative differences in reaction rates between plagioclase and K-feldspar weathering as well as in terms of differences in experimental and natural rates for the same feldspar.

Plagioclase and K-feldspar weathering are both kinetically controlled in the Davis Run regolith. Their relative reaction rates are directly proportional to the linear slopes describing their measured distributions with regolith depth (Fig. 10). A ratio of $k_{plag}/k_{Kspar} = 2.7$ for Davis Run indicates plagioclase weathers only slightly faster than K-feldspar. This is in agreement with similarities in rate data compiled in Table 10 and with the conclusions of Blum and Stillings (1995) who found little difference in the relative rates of experimental plagioclase and K-feldspar weathering at neutral to acidic conditions. The fact that the similarities in the relative rates of plagioclase to K-feldspar rates extend to natural conditions is consistent with the findings of Velbel (1993) who concluded that the ratios of reaction rates for different minerals are similar for natural and experimental weathering. These similarities imply that for the tabulated studies (Table 10), experimental and natural conditions were such that both plagioclase and K-feldspar weathering was sufficiently far from chemical equilibrium to be kinetically and not saturation controlled. However, many natural situations exist, such as in Panola bedrock weathering, where chemical saturation does occur for one of the feldspar phases, resulting in very large differences in the relative rates of plagioclase and K-feldspar weathering.

In terms of absolute rates for plagioclase and K-feldspar weathering, the data in Table 10 generally fall within two categories: relatively fast experimental dissolution rates determined using freshly crushed feldspars (k_r to 10^{-11} to 10^{-13} mol $m^{-2}s^{-1}$) and significantly slower natural weathering rates that exhibit significantly more variability ($k_r = 10^{-12}$ to 10^{-16} mol $m^{-2}s^{-1}$). The cause of some of this variability lies in differing methods used to determine mineral surface areas in the natural environment. The use of gas sorption isotherm

methods (BET) generally results in surface areas that are one to two orders of magnitude larger than for geometric estimates (White and Peterson, 1995; Brantley et al., 1999). This difference has the inverse effect on the weathering rate, with BET surface areas producing correspondingly slower rates (Table 10). Other causes for significant differences between laboratory and field rates include failures to reach steady-state linear reaction rates in short-term experiments, dilute experimental solutions vs. near-thermodynamically saturated natural waters, differences in wetted surface areas, and decreases in mineral surface reactivity with time (see reviews in White and Brantley, 1995).

Feldspar weathering rates for the Panola and Davis Run regoliths are among the slowest rates yet recorded for natural feldspar weathering. They are comparable only with rates based on solid-state elemental changes in the Merced soil chronosequence in California (Table 10). In that study (White et al., 1996), individual rates for plagioclase and K-feldspar weathering decreased by an order of magnitude from the youngest (10^3 yr) to the oldest (10^6 yr) soils. This trend was attributed to decreases in mineral reactivity with time as surface weathering reactions consume impurities, dislocations, and other crystallographic defects in feldspars (Lee et al., 1998). Likewise, increasing thicknesses of secondary clay and Fe-oxyhydroxide coatings exert a negative impact on dissolution rates by effectively shielding chemical interaction between the feldspar mineral surfaces and pore waters. Slow feldspar weathering rates in the geomorphically old Panola and Davis Run regoliths and the Merced soils are contrasted to much faster weathering rates for watersheds and soils that have undergone denudation by glaciation during the last 10 to 15 kyr (Table 10). The exposure of fresh bedrock during active physical erosion is expected to produce new, more reactive mineral surface, thus accelerating the weathering rates.

The large ranges in experimental and natural feldspar reaction rates have major implications in terms of predicted feldspar stabilities in granitic regoliths. For example, Wang et al. (1995) and Nahon and Merino (1997) used an extremely fast reaction rates (1×10^{-6} mol m^{-2} s^{-1}) to model Ca-plagioclase weathering in saprolite-laterite environments. This rate effectively dissolved 0.1- to 1-cm diameter plagioclase grains in time spans of tens to hundreds of years. If the average of the experimental rate data listed in Table 10 for plagioclase is used ($\log k_{plag} = 10^{-11.5}$ mol $m^{-2}s^{-1}$), the spreadsheet calculations (Table 8) predict that plagioclase grains are completely consumed in <10 kyr. In contrast, based on cosmogenic isotope age dates, plagioclase must persist in Panola and Davis Run regoliths for time periods approaching a million years. Clearly, the longevity of feldspars in these weathering environments must be reflected in much lower kinetic rates than provided by experimental studies. The slowness at which feldspars can react in selective weathering environments is often not fully recognized.

4.7. Differences in Weathering Environments

Most previous weathering studies of granite have focused on the unconsolidated part of the regolith. The pervasive nature of plagioclase weathering in the Panola bedrock is surprising considering the common assumptions concerning the impermeable nature of granite bedrock. Many aspects of the Panola and Davis Run regoliths are similar, including the initial minerals, the formation of saprolitic regoliths, and the time spans over which the weathering has occurred. Despite these similarities, basic differences must control the nature of bedrock vs. saprolite weathering in these regoliths.

The weathering rate of plagioclase in the Panola bedrock (2.8×10^{-16} mol m^{-2} s^{-1}) is approximately 7 times faster than the plagioclase rate in the Davis Run saprolite (4.0×10^{-17} mol $m^{-2}s^{-1}$). This is predicted on the basis of observations that both the propagation rate of the weathering front is more rapid and the slope of the plagioclase weathering profile is shallower in the Panola bedrock than in the Davis Run saprolite (Eqn. 14). A more rapid bedrock weathering rate is somewhat surprising based on hydrologic considerations because bedrock permeability is much lower than saprolite permeability (Table 9). A faster plagioclase weathering rate in the bedrock vs. saprolite environment implies that the weathering rates are not controlled by fluid transport rates as would be the case for chemically saturated conditions. The Panola plagioclase composition has a higher anorthite component (An_{23}) than does the Davis Run plagioclase (An_6). Experimental dissolution rates of plagioclase (Blum and Stillings, 1995) suggest that the oligioclase composition of the Panola Granite may weather a factor of 5 faster than the albite composition of the Occoquan Granite. This composition difference may also be manifested by the more rapid development of internal permeability in the Panola plagioclase as has been observed for calcic-rich cores of zoned plagioclases (Clayton, 1986).

Climate difference is another variable that affects feldspar weathering rates. The subtropical Panola watershed has an average annual precipitation of 1.24 m and an air temperature of 17°C. In contrast, the more temperate Davis Run watershed has a slightly less precipitation 1.04 m but a significantly lower temperature 10°C. White and Blum (1995) proposed a coupled equation that describes the effects of precipitation and temperature on chemical weathering rates. If the minor precipitation differences are neglected, then the expected temperature effect on the plagioclase reaction is

$$\frac{r_1}{r_0} = \exp\left[\frac{E_a}{R}\left(\frac{1}{T_0} - \frac{1}{T_1}\right)\right] \tag{15}$$

where r_1 and r_0 are the reaction rates at temperatures T_0 and T_1. R is the molar gas constant (8.31 J mol^{-1} $^0K^{-1}$), and E_a is the activation energy of the reaction (J mol^{-1}).

White et al. (1999b) experimentally investigated the weathering rate of the Panola granite as a function of temperature and calculated, based on Na and Si release, an average activation energy of 55 kJ mol^{-1}. This value is comparable with activation energies determined for experimental plagioclase dissolution (see review by Blum and Stillings, 1995). Substituting 55 kJ mol^{-1} for E_a into Eqn. 15, along with average temperatures for the Panola and Davis Run watersheds, produces an r_1/r_0 ratio of $\approx$2. Based solely on temperature differences, plagioclase weathering in the Panola Granite is about twice as fast as that at Davis Run. Compositional and temperature differences, discussed above, are sufficient to explain the fact that the Panola plagioclase weathering rate is a factor of 7 faster than Davis Run rate. This difference may explain, in part, the

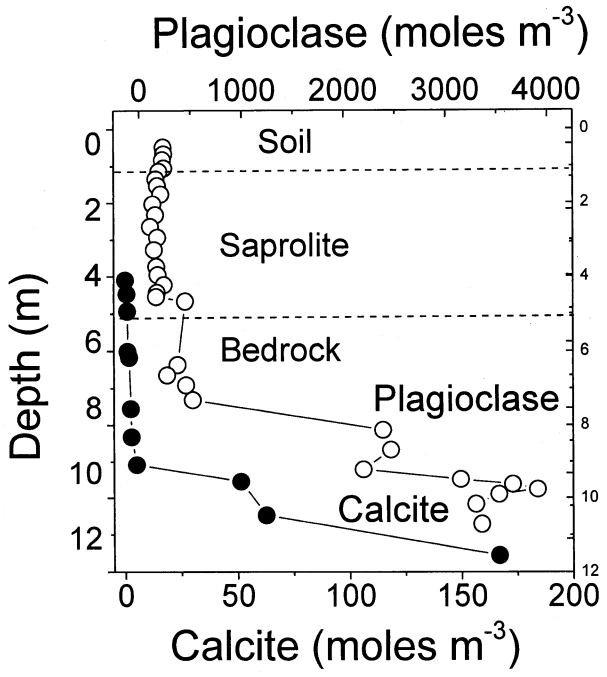

Fig. 13. Distributions of calcite (closed circles) and plagioclase (open circles) with depth in the Panola regolith.

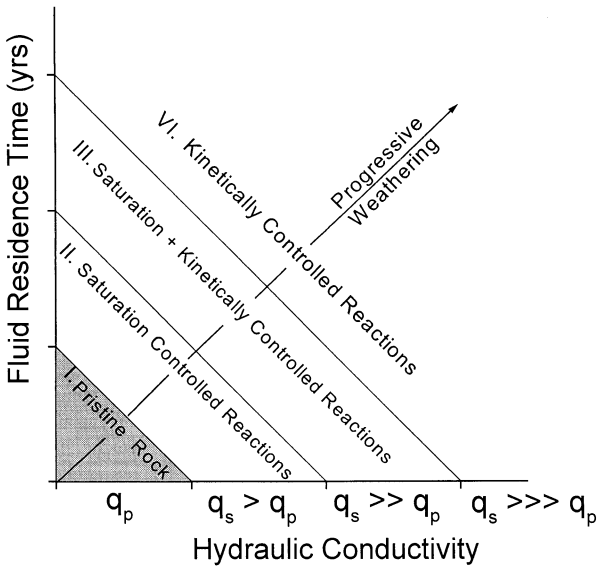

Fig. 14. Schematic diagram showing progressive weathering stages as functions of increasing weathering time and primary and secondary conductivities q_p and q_s.

extensive weathering of plagioclase in the Panola bedrock compared with the Davis Run bedrock.

The penetration of meteoric water into the pristine granite is required to initiate plagioclase weathering. One unique feature of the Panola granite is the relatively high content of disseminated calcite (0.33 wt.%) relative to most other granites (White et al., 1999b). Calcite occurs in the Panola Granite in relatively large interstitial grains as well as smaller inclusions along grain boundaries. The calcite content of the Occoquan Granite, by contrast, is much lower (0.07%; Seiders et al., 1975). As shown in experimental dissolution studies, calcite weathers out of the Panola Granite much faster than do silicate minerals (White et al., 1999b). This is substantiated by the presence of a calcite weathering front that precedes the plagioclase-weathering front by about a meter into the Panola Granite (Fig. 13). The close spatial correlation between weathering of the two phases with very different reactivities suggests initial transport-controlled bedrock weathering (Fig. 13). Petrographic evidence indicates the presence of relatively large, clay-lined vugs within the plagioclase phenocrysts that could have resulted from weathering out of disseminated calcite grains (Fig. 4B). The higher calcite content of Panola relative to most other granites could account for at least part of the difference in bedrock rock weathering rates.

4.8. Generalized Weathering Regimens

The spreadsheet model used to characterize feldspar weathering in the Panola and Davis Run regoliths uses rather simplistic assumptions concerning thermodynamic and kinetic controls on mineral reaction rates and the nature of hydrologic processes (Table 8). The exercise, however, provides a valuable framework that delineates different hydrochemical weathering environments in granitic regoliths (Fig. 14). Progressive isovolumetric granite weathering increases in the direction of the arrow along axes that define duration of weathering and the increase in hydraulic conductivity. Any point on the diagonal lines perpendicular to this weathering vector is equal to numerical product of time and hydraulic conductivity, which is equivalent to the volume of fluid that has passed through the regolith. Thus, weathering progress is defined in terms of increasing fluid volumes. The longer the time and/or the greater the conductivity, the larger will be the solution volume and the greater the extent of regolith weathering.

The diagonal lines defining solution volume enclose specific steps through which regolith weathering progresses (steps I–IV in Fig. 14). These steps correspond to sequential calculations in the spreadsheet (Table 8). The pristine granite exists below the penetration depth of the meteoric water-wetting front (step I). This condition exists because the primary hydraulic conductivity is too low (horizontal axis in Fig. 14 and/or the time interval is too short (vertical axis) for water to have penetrated into the bedrock. Once the wetting front moves through the pristine granite, weathering commences and fluids begin to transport reaction products from the granite, creating secondary permeability such that $q_s > q_p$ (step II). Under these conditions, the limited pore water rapidly saturates with respect to the reactive mineral phases. Weathering rates at this stage of regolith development are dependent on rates of fluid transport through the weathered granite rather than on the kinetic rates at which the primary minerals react.

With increasing time, continued mass transport increases the secondary conductivity, $q_s \gg q_p$, such that fluid pore volume becomes sufficiently large so that one or more of the most soluble reactive minerals becomes thermodynamically undersaturated (step III). Weathering of these minerals will now be dependent on their kinetic rate of reaction and not on the fluid transport rate defined by q_s. Mineral phases with lower solu-

bilities will continue to remain thermodynamically saturated. The Panola bedrock is consistent with this weathering regimen in which the plagioclase rate is kinetically controlled and the K-feldspar rate is saturation inhibited. An important characteristic of such heterogeneous weathering is that the relative rates of mineral weathering are more dependent on their respective solubilities than on their kinetic reaction rates. Finally, sufficient mass transfer occurs such that $q_s \ggg q_p$, which increases the pore water volume to the extent that all the primary minerals become unsaturated (step IV). In such a case, as in the highly permeable saprolite at Davis Run, the weathering of plagioclase and K-feldspar is directly proportional to their kinetic reaction rates.

5. CONCLUSIONS

A quantitative framework is developed in which to assess the chemical and hydrologic controls on feldspar weathering in granitic regoliths. Input data consist of detailed elemental and $^{87}Sr/^{86}Sr$ distributions in a deep soil-saprolite-bedrock regolith developed on the Panola Granite in Georgia, United States. Bulk density data, combined with trace distributions of Ti, Zr, and Nb, confirm isovolumetric regolith development. Mass balances indicate that Na and Ca are extensively mobilized in the weathered bedrock, K and Mg are mobilized in the overlying saprolite, and Fe and Al are mobilized in the soil. Petrographic data, combined with mineral compositions, show that these elemental distributions correspond to sequential losses of plagioclase in the bedrock, K-feldspar and biotite in the saprolite, and loss of Fe-oxides and kaolinite from the soil. The Panola results are contrasted to other regoliths in the eastern Piedmont, specifically, Davis Run in Virginia, which exhibits a lack of bedrock feldspar weathering, but extensive plagioclase and K-feldspar weathering in the overlying thick saprolite sequence.

A graphical extrapolation of ratios of $^{87}Sr/^{86}Sr$ vs. Nb/Sr shows that the increases in $^{87}Sr/^{86}Sr$ with depth in the bedrock are attributed to increasing residual plagioclase. Aqueous chemical speciation calculations show that the pore water compositions are bracketed by gibbsite and amorphous aluminum hydroxide saturation. This finding validates the use of measured total Al concentrations and reconstructed pH measurements to determine feldspar saturation states. Results show pore waters are thermodynamically undersaturated with albite but saturated with K-feldspar.

The above results are used to construct a weathering model that describes residual feldspar distributions in the granitic regoliths based on kinetic reaction rates, specific surface areas and primary and secondary hydraulic conductivities. Results of the model delineate sequential weathering environments that occur in stages: (I) the pristine granite in which the infiltrating front of meteoric water is controlled by the primary rock conductivity, (II) a zone of low secondary permeability in which plagioclase and K-feldspar are thermodynamically saturated and weathering rates are controlled by fluid transport, (III) a zone of moderate permeability in which K-feldspar weathering remains transport limited and plagioclase rates are kinetically controlled, and (IV) a zone of high permeability in which both plagioclase and K-feldspar are kinetically controlled.

The best fit of the model to feldspar profiles in the Panola bedrock produces comparable kinetic dissolution rates for plagioclase and K-feldspar that are in accord with similarities in experimentally rates determined under conditions far from chemical equilibrium. However, the moderate secondary permeability in the Panola bedrock (stage III) strongly suppresses K-feldspar weathering in accord with petrographic evidence showing pristine K-feldspars in contract with completely kaolinized plagioclase. Under such conditions, relative rates of feldspar weathering are more dependent on their respective solubilities than on their kinetic rate constants. The best fit of the model to the feldspar profiles in the Davis Run saprolite denote high permeability weathering (stage IV) in which plagioclase and K-feldspar distributions are directly dependent on their respective kinetic rate constants. Faster plagioclase reaction, leading to bedrock weathering in the Panola Granite but not at Davis Run, is attributed to a higher anorthite component, a wetter and warmer climate, and larger amounts of disseminated calcite, the reaction of which leads to a greater bedrock permeability.

Acknowledgments—This work was funded under the auspices of the Water, Energy, and Biogeochemical Budgets Program of the U.S. Geological Survey. The authors thank Bret Aulenbach for field assistance and John Fitzpatrick, Davison Vivit, and Steve Newton for laboratory assistance. Rick Hooper and Doug Burns of the USGS also contributed useful insights. The authors also thank Drs. Robert Berner, Susan Brantley, and an anonymous reviewer for helpful review comments.

Associate editor: D. L. Sparks

REFERENCES

Abelin H., Birgerrson L., Moreno L., Widen H., Agen T., and Neretnieks I. (1991) A large-scale flow and tracer experiment in granite: Results and interpretation. *Water Resources Res.* **27,** 3119–3135.

Arth J. (1976) Behavior of trace elements during magmatic processes—A summary of theoretical models and their applications. *J. Res. U.S. Geol. Surv.* **4,** 41–47.

Banfield J. F. and Eggleton R. A. (1990) Analytical transmission electron microscope studies of plagioclase and K-feldspar weathering. *Clays Clay Minerals* **38,** 77–89.

Beavis F. C. (1985) *Engineering Geology*. Blackwell Scientific, 356 p.

Berner R. A. and Berner E. K. (1997) Silicate weathering and climate. In *Tectonic Uplift and Climate Change* (ed. W. F. Ruddiman), pp. 353–364. Plenum Press.

Bierman P., Gillespie A., Caffee M., and Elmore D. (1995) Estimating erosion rates and exposure ages with ^{36}Cl produced by neutron activation. *Geochim. Cosmochim. Acta* **59,** 3779–3798.

Blum A. E. and Stillings L. L. (1995) Feldspar dissolution kinetics. In *Chemical Weathering Rates of Silicate Minerals*, pp. 291–338 (ed. A. F. White and S. L. Brantley). Mineralogical Society of America.

Brady P. V. and Carroll S. A. (1994) Direct effects of CO_2 and temperature on silicate weathering: Possible implications for climate control. *Geochim. Cosmochim. Acta* **58,** 1853–1863.

Brantley S. L. (1992) Kinetics of dissolution and precipitation—Experimental and field results. In *Proceedings of the 7th International Symposium on Water-Rock Interaction* (ed. Y. K. Kharaka and A. S. Maest), pp. 85–88. Balkema.

Brantley S. L., Chesley J. T., and Stillings L. L. (1998) Isotopic ratios and release rates of strontium measured from weathering of feldspars. *Geochim. Cosmochim. Acta* **62,** 1493–1500.

Brantley S. L., White A. F., and Hodson M. E. (1999) Surface areas of primary silicate minerals. In *Growth, Dissolution and Pattern Formation in Geosystems* (ed. B. Jamtveit and P. Meakin), pp. 291–326. Kluwer Academic Publishers.

Brimhall G. H. and Dietrich W. E. (1987) Constitutive mass balance

relations between chemical composition, volume, density, porosity, and strain in metasomatic hydrochemical systems: Results on weathering and pedrogenesis. *Geochim. Cosmochim. Acta* **51,** 567–587.

Brimhall G. H., Lewis C. J., Ford C., Bratt J., Taylor G., and Warin O. (1991) Quantitative geochemical approach to pedogenesis: Importance of parent material reduction, volumetric expansion, and eolian influx in lateritization. *Geoderma* **51,** 51–91.

Bryon D. N., Atherton M. P., and Hunter R. H. (1995) The interpretation of granitic textures from serial thin sectioning, image analysis and three dimensional reconstruction. *Mineral. Mag.* **59,** 203–211.

Bullen T. D., White A. F., Blum A. E., Harden J. W., and Schulz M. S. (1997) Chemical weathering of a soil chronosequence on granitoid alluvium. II. Mineralogic and isotopic constraints on the behavor of strontium. *Geochim. Cosmochim. Acta* **61,** 291–306.

Bullen T. D., White A. F., Huntington T. G., and Peters N. E. (1999) A new approach for determining the $^{87}Sr/^{86}Sr$ ratio of the "granitoid" weathering component. *Proceedings of Geochemistry of the Earth's Surface,* pp. 369–372. Reykjavik.

Buol S. W. and Weed S. B. (1991) Saprolite-soil transformations in the Piedmont and Mountains of North Carolina. *Geoderma* **51,** 15–28.

Burch T. E., Nagy K. L., and Lasaga A. C. (1993) Free energy dependence of albite dissolution kinetics at 80°C, and pH 8.8. *Chem. Geol.* **105,** 137–162.

Burns D. A. (1998) The hydrochemical evolution of stormflow in a forested Piedmont catchment. PhD thesis, College of Environmental Sciences and Forestry State Uni. New York, 261 p.

Busenberg E. and Clemency C. V. (1976) The dissolution kinetics of feldspars at 25°C and 1 atm. CO_2 partial pressure. *Geochim. Cosmochim. Acta* **40,** 41–49.

Calvert C. S., Buol S. W., and Weed S. B. (1980) Mineralogical characteristics and transformations of a vertical rock-saprolite-soil sequence in the North Carolina Piedmont. I. Profile morphology, chemical composition and mineralogy. *Soil Sci. Am. J.* **44,** 1096–1103.

Chadwick O. A., Brimhall G. H., and Hendricks D. M. (1990) From black box to a grey box: A mass balance interpretation of pedogensis. *Geomorphology* **3,** 369–390.

Clayton J. L. (1986) An estimate of plagioclase weathering rate in the Idaho Batholith based upon geochemical transport rates. In *Rates of Chemical Weathering of Rocks and Minerals* (ed. S. Coleman and D. Dethier), pp. 453–466. Academic Press.

Chou L. and Wollast R. (1985) Steady-state kinetics and dissolution mechanisms of albite. *Am. J. Sci.* **285,** 963–993.

Cleaves E. T. (1993) Climatic impact on isovolumetric weathering of a coarse-grained schist in the northern Piedmont Province of the central Atlantic states. *Geomorphology* **8,** 191–198.

Clow D. W. and Drever J. I. (1996) Weathering rates as a function of flow through an alpine soil. *Chem. Geol.* **132,** 131–141.

Farver J. R. and Yund R. A. (1993) Grain boundary diffusion in feldspar aggregates. *EOS Trans. Amer. Geophys. Union* **74,** 610–611.

Galle C. (1994) Neutron porosity logging and core porosity measurements in the Beauvoir Granite, Massif Central Range, France. *J. Appl. Geophys.* **32,** 125–137.

Gardner L. R. (1980) Mobilization of Al and Ti during weathering-isovolumetric geochemical evidence. *Chem. Geol.* **30,** 151–165.

Grant W. H. (1963) Weathering of Stone Mountain Granite. *Clays Clay Minerals* **13,** 65–73.

Grant W. H. (1975) Chemical Weathering of Panola Adamellite with special reference to apatite. *Southeastern Geol.* **17,** 15–25.

Graustein W. C. and Armstrong R. L. (1983) The use of strontium-87/stronium-86 ratios to measure atmospheric transport in forested watersheds. *Science* **219,** 289–292.

Harden J. W. (1987) Soils Developed in Granitic Alluvium near Merced, California. *U.S. Geol. Surv. Bull.* **1590-A**. 65 p.

Higgins M. W., Atkins R. L., Crawford T. J., Crawford R. F. III, Brooks R., and Cook R. (1988) The structure, stratigraphy, tectnostratigraphy and evolution of the southern most part of the Appalachian orogen. *U.S. Geol. Surv. Prof. Paper* **1475,** 173.

Holdren G. R., Jr., and Speyer P. M. (1985) pH dependent changes in the rates and stoichiometry of dissolution of an alkali feldspar at room temperature. *Am. J. Sci.* **285,** 994–1019.

Huntington T. G., Hooper R. P., Johnson C. E., Aulenbach B. T., Cappellato R., and Blum A. E. (2000). Calcium depletion in forest ecosystems of the southeastern United States. *Soil Sci. Soc. Am. J.* **64,** 1845–1858.

Johnson N. M., Likens G. E., Bormann F. H., and Pierce R. S. (1968) Rate of chemical weathering of silicate minerals in New Hampshire. *Geochim. Cosmochim. Acta* **32,** 531–545.

Kenoyer G. J. and Bowser C. J. (1992) Groundwater chemical evolution in a sandy silicate aquifer in Northern Wisconsin 2. Reaction modeling. *Water Resources Res.* **28,** 591–600.

Kirkwood D. E. and Nesbitt, H. W. (1991) Formation and evolution of soils from an acidified watershed: Plastic Lake, Ontario, Canada. *Geochim. Cosmochim. Acta* **55,** 1295–1308.

Knauss K. G. and Wolery T. J. (1986) Dependence of albite dissolution kinetics on pH and time at 25°C and 70°C. *Geochim. Cosmochim. Acta* **50,** 2481–2497.

Kretzschmar R. W., Robarge P., Amoozegar A., and Vepraskas M. J. (1997) Biotite alternation to halloysite and kaolinite in soil-saprolite profiles developed for mica schist and granite gneiss. *Geoderma* **75,** 155–170.

Lasaga A. C. (1984) Chemical kinetics of water-rock interaction. *J. Geophys. Res.* **89,** 4009–4025.

Lee M. R., Hodson, M E., and Parsons I. (1998) The role of intragranular microtextures and microstructures in chemical and mechanical weathering: Direct comparisons of experimentally and naturally weathered alkali feldspars. *Geochim. Cosmochim. Acta* **62,** 2771–2788.

Markewich H. W. and Pavich M. J. (1991) Soil chronosequence studies in temperate to subtropical, low-latitude, low-relief terrain with data from the eastern United States. *Geoderma* **51,** 213–239.

Mast M. A. and Drever J. I. (1987) The effect of oxalate on the dissolution rates of oligoclase and tremolite. *Geochim. Cosmochim. Acta* **51,** 2559–2568.

Merino E., Nahon, D., and Wang, Y. (1993) Kinetics and mass transfer of pseudomorphic replacement: Application to replacement of parent minerals and kaolinite by Al, Fe and Mn oxides during weathering. *Am. J. Sci.* **293,** 135–155.

Montgomery C. W. and Brace W. F. (1975) Micropores in plagioclase. *Contrib. Mineral. Petrol.* **52,** 17–28.

Morrow C. A. and Lockner D. A. (1997) Permeability and porosity of the Illinois UPH 3 drillhole granite and a comparison with other deep drillhole rocks. *J. Geophys. Res.* **102 B2,** 3067–3075.

Mosquera M. J., Rivas T., Prieto B., and Silva B. (2000). Capillary rise in granitic rocks: Interpretation of kinetics on the basis of pore structure. *J. Colloid Interface Sci.* **222,** 41–45.

Nagy K. L. and Giletti B. J. (1986) Grain boundary diffusion of oxygen in macroperthitic feldspar. *Geochim. Cosmochim. Acta* **50,** 1151–1158.

Nahon D. and Merino, E. (1997) Pseudomorphic replacement in tropical weathering: Evidence, geochemical consequences and kinetic-rheological origin. *Am. J. Sci.* **297,** 393–417.

Nesbitt H. W., Fedo C. M., and Young G. M. (1997) Quartz and feldspar stability, steady and non-steady state weathering and petrogenesis of siliciclastic sands and muds. *J. Geol.* **105,** 173–191.

Nixon R. A. III. (1981) Rates and mechanisms of chemical weathering in an organic environment at Panola Mountain. MS thesis, Georgia, Emory Univ., 265 p.

Oelkers E. H., Schott J., and Devidal J. L. (1994) The effect of aluminum, pH, and chemical affinity on the rates of alumino-silicate dissolution reactions. *Geochim. Cosmochim. Acta* **58,** 2011–2024.

Oxburgh R., Drever J. I., Sun Y. T. (1994) Mechanism of plagioclase dissolution in acid solutions at 25°C. *Geochem. Cosmochem. Acta* **58,** 661–669.

Paces T. (1986) Rates of weathering and erosion derived from mass balance in small drainage basins. In *Rates of Chemical Weathering of Rocks and Minerals* (ed. S. M. Colman and D. P. Dethier), pp. 531–550. Academic Press.

Parkhurst D. L. (1997) Geochemical mole-balance modeling with uncertain data. *Water Resources Res.* **33,** 1957–1970.

Pavich M. J. (1986) Processes and rates of saprolite production and erosin on a foliated granitic rock of the Virgina Piedmont. In *Rates of Chemical Weathering of Rocks and Minerals* (ed. S. M. Colman and D. P. Dethier), pp. 551–590. Academic Press.

Pavich M. J., Brown L., and Valette-Silver H. N. (1995) ^{10}Be analysis

of a quaternary weathering profile in the Virginia Piedmont. *Geology* **13,** 39–41.
Pavich M. J., Leo G. W., Obermeier S. F., and Estabrook J. R. (1989) Investigations of the characteristics, origin, and residence time of the upland residual mantle of the Piedmont of Fairfax County, Virginia. *U. S. Geol. Surv. Prof. Paper* **1352,** 58.
Philpotts A. R., Brustman C. M., Shi J., Carlson W. D., and Denison C. (1999) Plagioclase-chain networks in slowly cooled basaltic magma. *Amer. Mineral.* **84,** 1819–1829.
Schnoor J. L. (1990) Kinetics of chemical weathering: A comparison of laboratory and field rates. In *Aquatic Chemical Kinetics* (ed. W. Stumm), pp. 475–504. J. Wiley and Sons.
Schoenberger P. J., Amoozegar A., and Buol S. W. (1995) Physical property of a soil and saprolite continuum at three geomorphic positions. *Soil Sci. Soc. Am.* **59,** 1389–1397.
Schroeder P. A. and Melear N. D. (1999) Stable carbon isotope signatures preserved in authigenic gibbsite from a forested granitic-regolith: Panola Mt. Georgia, USA. *Geoderma* **91,** 261–279.
Schweda P. (1989) Kinetics of alkali feldspar dissolution at low temperature. In *Proc. 6th Intern. Symp. Water/Rock Interaction* (ed. D. L. Miles), pp. 609–612. A. A. Balkema.
Seiders V. M., Mixon R. B., Stern T. W., Newell M. F., and Thomas C. B. J. (1975) Age of plutonism and tectonism and a new minimum age limit on the Glenarm series in the northeast Virginia Piedmont near occoquan. *Am. J. Sci.* **275,** 481–499.
Siegel D. and Pfannkuch H. O. (1984) Silicate mineral dissolution at pH 4 and near-standard temperature and pressure. *Geochim. Cosmochim. Acta* **48,** 197–201.
Stauffer R. E. (1990) Granite weathering and the sensitivity of alpine lakes to acid deposition. *Limnol. Oceangr.* **35,** 1112–1134.
Stillings L. L., Drever J. I., Brantley S. L., Sun Y. T., and Oxburgh, R. (1996) Rates of feldspar dissolution at pH 3–7 with 0–8 M oxalic acid. *Chem. Geol.* **132,** 79–89.
Stonestrom D. A., White A. F., and Akstin K. C. (1998) Determining rates of chemical weathering in soils-solute transport versus profile evolution. *J. Hydrol.* **209,** 331–345.
Suarez D. L. and Wood J. D. (1996) Short-term and long term weathering rates of a feldspar fraction isolated from an arid zone soil. *Chem. Geol.* **132,** 143–150.
Sverdrup H. U. (1990) *The Kinetics of Base Cation Release Due to Chemical Weathering.* Lund University.
Swoboda-Colberg N. G. and Drever J. I. (1992) Mineral dissolution rates: A comparison of laboratory and field studies. In *Proc. 7th Intern. Symp. Water-Rock Interaction* (ed. Y. K. Kharaka and A. S. Maest), pp. 115–117. Balkema.
Van Tassel J. V. and Grant W. H. (1980) Granite disintegration, Panola Mountain, Georgia. *J. Geol.* **88,** 360–364.
Velbel M. A. (1985) Geochemical mass balances and weathering rates in forested watersheds of the southern Blue Ridge. *Am. J. Sci.* **285,** 904–930.
Velbel M. A. (1990) Mechanisms of saprolitization, isovolumetric weathering and pseudomorphic replacement during rock weathering-A review. *Chem. Geol.* **84,** 17–19.
Velbel M. A. (1993) Consistency of silicate-mineral weathering rate ratios between natural and experimental weathering: implications for hydrologic control of differences in absolute rates. *Chem. Geol.* **105,** 89–99.
Vepraskas M. J. and Williams J. P. (1995) Hydraulic conductivity of saprolite as a function of sample dimensions and measurement technique. *Soil Sci. Am. J.* **59,** 975–981.
Wang Y., Wang H., and Merino E. (1995) Dynamic weathering model: Constraints required by coupled dissolution and pseudomorphic replacement. *Geochim. Cosmochim. Acta* **59,** 1559–1570.
Welch S. A. and Ullman W. J. (1996) Feldspar dissolution in acidic and organic solutions: Compositional and pH dependence of dissolution rate. *Geochim. Cosmochim. Acta* **60,** 2939–2948.
White A. F. (1995) Chemical weathering rates in soils. In *Chemical Weathering Rates of Silicate Minerals* (eds. A. F. White and S. L. Brantley), Vol. 31, pp. 407–458. Mineralogical Soc. Am.
White A. F. and Peterson M. L. (1990) Role of reactive surface area characterization in geochemical models. In *Chemical Modeling of Aqueous Systems II* (eds. D. C. Melchior and R. L Basset), Vol. 416, pp. 461–475. ACS Symp. Ser.
White A. F. and Blum A. E. (1995) Effects of climate on chemical weathering rates in watersheds. *Geochim. Cosmochim. Acta* **59,** 1729–1747.
White A. F. and Brantley S. L. (1995) Chemical weathering rates of silicate minerals. In *Reviews in Mineralogy*, Vol. 31, pp. 584. Mineralogical Society of America.
White A. F., Blum A. E., Schulz M. S., Bullen T. D., Harden J. W., and Peterson M. L. (1996) Chemical weathering of a soil chronosequnece on granitic alluvium. I. Reaction rates based on changes in soil mineralogy. *Geochim. Cosmochim. Acta* **60,** 25333–2550.
White A. F., Blum A. E., Schulz M. S., Vivit D. V., Larsen M., and Murphy S. F. (1998) Chemical weathering in a tropical watershed, Luquillo Mountains, Puerto Rico. I. Long-term versus short-term chemical fluxes. *Geochim. Cosmochim. Acta* **62,** 209–226.
White A. F., Bullen T. D., Vivit D. V., and Schulz M. S. (1999a) The role of disseminated calcite in the chemical weathering of granitoid rocks. *Geochim. Cosmochim. Acta* **63,** 1939–1953.
White A. F., Blum A. E., Bullen T. D., Vivit D. V., Schulz M., and Fitzpatrick J. (1999b) The effect of temperature on experimental and natural weathering rates of granitoid rocks. *Geochim. Cosmochim. Acta* **63,** 3277–3291.
White A. F., Blum A. E., Stonestrom D. A., Bullen T. D., Schulz M. S., Huntington T. G., and Peters N. E. (2001). Chemical weathering of the Panola Granite: Solute and regolith fluxes and the weathering rate of biotite. In *Water-Rock Interaction, Ore Deposits, and Environmental Geochemisty: A Tribute to David A. Crerar* (eds. R. Hellmann and S. A. Wood. Geochemical Society (in press).
Zhao J. (1998) Rock mass hydraulic conductivity of the Bukit Timah granite, Singapore. *Eng. Geol.* **50,** 211–216.